NONINVASIVE BRAIN PATHOLOGY MONITORING USING CONDUCTIVITY MEASUREMENT: A SIMULATION STUDY

PRACHA YAMBANGYANG

A THESIS SUBMITTED IN PARTIAL FULFILLMENT
OF THE REQUIREMENTS FOR
THE DEGREE OF MASTER OF ENGINEERING
(BIOMEDICAL ENGINEERING)
FACULTY OF GRADUATE STUDIES
MAHIDOL UNIVERSITY
2005

ISBN 974-04-5966-8

Thesis
Entitled

NONINVASIVE BRAIN PATHOLOGY MONITORING USING CONDUCTIVITY MEASUREMENT: A SIMULATION STUDY

P. Yambangyang
.....
Mr. Pracha Yambangyang
Candidate

.....
Asst.Prof.Chatchai Neatpisarnvanit,
Ph.D. (Electrical Engineering)
Major-Advisor

.....
Mr. Nanthasak Tisavipat,
M.D. Grad Dip in Clin Sc (Surg)
Co-Advisor

Rassmidara Hoonsawat
.....
Assoc.Prof.Rassmidara Hoonsawat,
Ph.D.
Dean
Faculty of Graduate Studies

Theeraporn Rubcumintara
.....
Asst.Prof. Theeraporn Rubcumintara,
Ph.D. (Materials Engineering & Science)
Chair
Master of Engineering
Program in Biomedical Engineering
Faculty of Engineering

Thesis
Entitled

NONINVASIVE BRAIN PATHOLOGY MONITORING USING CONDUCTIVITY MEASUREMENT: A SIMULATION STUDY

was submitted to the Faculty of Graduate Studies, Mahidol University
For the degree of Master of Engineering (Biomedical Engineering)
on
1 April, 2005

.....
Mr. Pracha Yambangyang
Candidate

.....
Asst.Prof.Chatchai Neatpisarnvanit,
Ph.D. (Electrical Engineering)
Chair

.....
Mr. Nanthasak Tisavipat,
M.D. Grad Dip in Clin Sc (Surg)
Member

.....
Asst.Prof. Udom Tipayamontri,
Ph.D. (Physiology)
Member

.....
Mr. Kriskrai Sitthiseripratip,
D. Eng (Manufacture Engineering System)
Member

.....
Assoc.Prof.Rassmidara Hoonsawat,
Ph.D.
Dean
Faculty of Graduate Studies
Mahidol University

.....
Asst.Prof. Piya Rattanasuwan,
M. Eng (Civil Engineering)
Dean
Faculty of Engineering
Mahidol University

ACKNOWLEDGEMENT

This thesis is supported in part by the Ministry of University Affairs and Faculty of Graduate Studies, Mahidol University in the academic year of 2003

I would like to express my sincere gratitude and deep appreciation to Dr. Chatchai Neatpisarnvanit, my major advisor, for warm attention, expect guidance, valuable advice, English writing correction, supervision and encouragement throughout. He has never been lacking in kindness and support. I am equally grateful to Mr. Nantasak Tisavipa, my co-advisor, for his constructive comments, supervision, encouragement, and providig the patient data.

I would like to express my deep gratitude to Mr. Kriskrai Sitthiseripratip, National Metal and Materials Technology Center (MTEC). for valuable advice, helpful guidance, suggestion and also supporting in this research.

I am gratefully thank to Mr. Arthorn Sanpanich for his helpful advice and support.

I wish to thank the staff of Biomedical Engineering Department, Faculty of Engineering, Mahidol University for their co-operation and generous assistance.

Special thank are extended to all subjects who participation made this study possible. It is my pleasure to thank my family members, all of my friends, which their names are not listed here but everyone is in my mind, for their love, helpful and everything they have done for me.

Pracha Yambangyang

NONINVASIVE BRAIN PATHOLOGY MONITORING USING CONDUCTIVITY MEASUREMENT: A SIMULATION STUDY

PRACHA YAMBANGYANG 4336837 EGBE/M

M.Eng. (BIOMEDICAL ENGINEERING)

THESIS ADVISORS: CHATCHAI NEATPISARNVANIT, Ph. D. (ELECTRICAL ENGINEERING), NANTHASAK TISAVIPA MD, Grad Dip in Clin Sc (Surg)

ABSTRACT

The purpose of this study was to predict a potential distribution of edema on a human head model with an edema condition. Brain edema is a clinical problem associated with the fluid accumulation in the brain tissue. The fluid's volume variation has an immediate effect on the conductivity of tissue, which can be measured by an electric impedance technique. This work aimed to apply finite element methods (FEM) to predict the current density distribution and electric potential distribution in the swelling brain when applying electric current through the brain via a pair of surface electrodes. Suitable locations of surface electrodes (used for picking up the measured electric potential from and applying current to the scalp) were studied extensively in this work. Electrical impedance measurement equipment, tissue-equivalent material and phantom were designed to validate the result obtained from the FEM simulation.

The obtained results indicate that more than 85 % of electric potential is attenuated through the skull. Furthermore, electric potential distribution in brain edema is found to be asymmetric and depends on locations of the swelling region. Simulation results show that the current applying electrodes should be placed nearby the swelling region. The validation results confirm that the edema lump causes reduction in the electric potentials.

KEY WORDS: BRAIN EDEMA/ CONDUCTIVITY/ FINITE ELEMENT METHOD

68 P. ISBN 974-04-5966-8

การเฝ้าระวังสภาวะความเป็นโรคสมองแบบไม่รุกล้ำโดยใช้ความนำทางไฟฟ้า: การศึกษาโดยใช้แบบจำลอง (NONINVASIVE BRAIN PATHOLOGY MONITORING USING CONDUCTIVITY MEASUREMENT: A SIMULATION STUDY)

ประชา แย้มบางยาง 4336837 EGBE/M

วศ.ม.(วิศวกรรมชีวการแพทย์)

คณะกรรมการควบคุมวิทยานิพนธ์ : ฉัตรชัย เนตรพิศาลวนิช Ph.D.(Electrical Engineering), นันทศักดิ์ ทิศาวิภาต MD. Grad Dip in Clin Sc (Surg)

บทคัดย่อ

การศึกษานี้มีวัตถุประสงค์เพื่อหาการกระจายของศักย์ไฟฟ้าของแบบจำลองของศีรษะที่ สมองบวมน้ำ สภาวะการบวมน้ำของสมองเป็นปัญหาทางการแพทย์ที่มีความสัมพันธ์กับการเพิ่มขึ้นของสารน้ำในสมอง การเปลี่ยนแปลงของปริมาณสารน้ำจะส่งผลต่อค่าความนำไฟฟ้าของเนื้อเยื่อโดยตรง และสามารถวัดค่าได้โดยวิธีวัดค่าอิมพีแดนซ์ ในการศึกษานี้ใช้ระเบียบวิธีไฟไนต์เอลิเมนต์สำหรับหาการกระจายของศักย์ไฟฟ้าบนศีรษะที่มีสภาวะการบวมน้ำ เมื่อทำการจ่ายกระแสไฟฟ้าผ่านทางคู่อิเล็กโทรด ในการศึกษายังทำการหาตำแหน่งที่เหมาะสมสำหรับการวางอิเล็กโทรดคู่ที่ใช้สำหรับวัดการกระจายของศักย์ไฟฟ้า นอกจากนั้นได้ทำการออกแบบเครื่องวัดอิมพีแดนซ์ เนื้อเยื่อจำลอง และ ศีรษะจำลอง เพื่อใช้ในการตรวจสอบผลที่ได้จากการวิเคราะห์จากระเบียบวิธีไฟไนต์เอลิเมนต์

จากผลที่ได้รับพบว่าค่าศักย์ไฟฟ้ามากกว่า 85% จะถูกลดทอนโดยกะโหลกศีรษะ นอกจากนั้นยังพบว่าการกระจายของศักย์ไฟฟ้าบนสมองเกิดความไม่สมมาตรเนื่องมาจากสภาวะการบวมน้ำ และการวางอิเล็กโทรดสำหรับจ่ายกระแสไฟฟ้าใกล้กับตำแหน่งมีการบวมน้ำจะมีความเหมาะสมสำหรับการวัด นอกจากนี้ผลการตรวจสอบจากแบบจำลองยังช่วยยืนยันว่าก้อนน้ำเป็นสาเหตุที่ทำให้การกระจายของศักย์ไฟฟ้าลดลง

68 หน้า ISBN 974-04-5966-8

CONTENTS

LIST OF TABLES

LIST OF FIGURE

LIST OF FIGURE (CONT.)

LIST OF FIGURE (CONT.)

LIST OF ABBREVIATIONS

Ag/AgCl	Silver / Silver Chlorine
CAD	Computer-aided design
CBF	Cerebral blood flow
CSF	Cerebrospinal fluid
CT	Computer tomography
DICOM	Digital imaging and communications in medicine
EIT	Electric impedance tomography
EEG	Electroencephalogram
FEA	Finite element analysis
FEM	Finite element method
ICP	Intracranial pressure
I/O	Input and Output
MRI	Magnetic resonance imaging
MUX	Multiplexer
VCCS	Voltage controlled current source
V/I	Voltage to current
SAR	Specific absorption rate

CHAPTER I
INTRODUCTION

1.1 Introduction

Normally, brain tissue is contained in the skull that is a rigid volume. The skull has a volume about 1650 ml, which consists of 150 ml blood volume, the 150 ml cerebrospinal fluid (CSF) and another fluid (1). When the brain volume increases, it will be compensated by decreasing the CSF volume but this compensation is limited at certain value. For example, when the brain tissue is bleeding (Hematoma), the pressure called intracranial pressure (ICP) will increase and cause a cerebral ischemia that is dangerous to the patient.

ICP may be elevated during microgravity due to a fluid shift in the head. As widely observed in clinical settings, elevated ICP causes headache, nausea and projectile vomiting, which are similar to symptoms of space adaptation syndrome. Elevated ICP may also comprise cerebral circulation and also be used as a sign of neurological deterioration in the management of patients with head trauma, cerebrovascular diseases, and brain tumors.

The ICP level can be described by the mechanism of formation, storage, and absorption of CSF. For under normal conditions the rate of formation is equally balanced by a rate of absorption which results in the zero storage components. Thus, both the resting CSF volumes remain unchanged. When the CSF volumes are changed, the CSF pressure will increase. The changing of CSF volumes affects the intracranial pressure level. This relationship is exponentially related.

Conventional methods for ICP monitoring require surgical procedures which are accompanied by an increased risk of infection. For this reason, candidates for ICP monitoring are currently only patients with severe neurological conditions. A noninvasive technique could make it possible to monitor ICP more easily and repeatedly in patients with a variety of neurosurgical conditions, thus aiding clinical

management and reducing the mortality and morbidity related to neurological diseases.

In the past, ICP monitoring was performed by invasive methods, such intraventricular device that used the catheter inserted into intraventricular in the brain. The transducer built-in at the tip of catheter converts the pressure to an electrical signal. This signal is conditioned by signal conditioning circuit before being transmitted to recorder. However, the drawbacks are that they required surgery and increase risk of infection. For this reason, non-invasive method becomes necessary to monitoring ICP.

Transcranial doppler ultrasonic is a noninvasive technique, which can measure the cerebral blood flow (CBF). That is a significant rise or fall of ICP. However, the doppler velocities may be altered by several factors, including the angle of insonation of the artery, the diameter of the vessel and variables that influence CBF. Moreover, this method is expensive, especially the ultrasonic transducer.

Bioelectrical impedance measurement is quick, portable and inexpensive. Impedance is inversely proportional to the volume of the conductor through which a current passes (2). Bioelectrical impedance is widely used to investigate volume changed. The movement of thorax during respired can be measurement by impedance for monitoring the respiratory system in adult and neonates (3). The body fat and fluid can also determined by impedance (4). Pressure and volume within the cardiac chamber is important for cardiovascular system. The intracardiac volume can be assessed by means of the impedance (5). Moreover, the impedance can be applied to measure the cerebral edema resulted from the failure of osmoregolation (2)

The relationship between pressure and impedance is indirect (6). The changed volume of brain tissue generates pressure. The result of these changing also causes changing of tissue’s conductivity properties. The pressure may be related to these properties. The brain’s resistivity variation can be measured in term of impedance by applying a current between 1 - 2.5 mA at 50 kHz, and two electrodes recorded voltage. When the current is applied through brain, 15% of the applied current entered the skull (7). Therefore, the skull not only attenuates the amount of applied current, but also reduces the signal from an expected impedance change in the human brain. In brief impedance measurement has many parameters such as current density distributions,

electric field amplitude and thickness of tissue layer and also the position of placing electrode is important for measuring.

In biomedical research, the finite element analysis (FEA) technique is an effective numerical tool for the design and analysis of engineering components. The FEA has been used widely to study and analysis of bioelectric signal phenomena and tissue properties in human. Finite Element Analysis or FEA minimizes the problem of the lack of specimen for in vitro testing or in the situation that requires the complicated preparation of the experiment.

The purpose of this study is to apply finite element to predict the current density distributions in brain pathophysiology when injecting the alternating current, which is done on multi-conductivity layer tissue model and also to determine the suitable position placement of electrodes for conductivity measurement. The simulation results will be verified by a series of phantom based experiments.

1.2 Objective

1.2.1 To predict a current density distribution and an electric field in brain using multi-conductivity layer tissue model and finite element method.

1.2.2 To determine suitable placement of electrodes for conductivity measurement in brain pathology.

1.2.3 To validate the results of finite element method by using a phantom model.

1.3 Scope of Project

1.3.1 3D model of brain is constructed from CT or MRI images. Then define a conductivity property of each layer and constructs a mesh of the model.

1.3.2 Maxwell’s equations are applied to the model to investigate and analyze current distribution in brain.

1.3.3 The proposed model will be applied to the brain pathology, such as edema and hematoma. The model will also be used to determine a suitable placement of electrodes for current distribution measurement in brain.

13.4 The results of finite element method will be validated by using electric impedance measurement and phantom.

1.4 Expected Results

This thesis proposes a development of a finite element method to determine the current distribution in brain pathology. The results of study involve a current distribution, electrical field distribution and electrical potential of each position on the model, which can be applied to design suitable instrument for tissue's conductivity or impedance measurement. A suitable position can be selected to place electrodes for measurements.

This model will be applied to two types of brain pathology (edema or hematoma) to investigate the current distribution under multi-conductivity tissue layer. Detection of fluid (or pressure) in brain using non-invasive bioelectric (impedance) measurement can be realized from the proposed model.

CHAPTER II
LITERATURE REVIEW

This chapter is divided into four parts: intracranial pressure (ICP), electrical properties of tissue, finite element method and review of related works. The intracranial pressure section will describe methods to monitoring ICP with a relationship between ICP and volume. Then, electrical volume conductivity section will be described the basic concept of conductivity and resistivity of biological tissues. The basic of finite element method and review of related works will be explained in the last section.

2.1 Intracranial Pressure (ICP)

2.1.1 Normal ICP wave

The ICP wave consists of respiratory and cardiac pulse as shown in Figure 2.1. In normal patients, ICP will be less than 15 mmHg; normal recording is 5-15 mmHg. When the ICP increases to 15-20 mmHg it is in the mild degree range. The moderate degree is 20-40 mmHg and more than 40 mmHg is severe.The ICP waves, due to the changes in systemic blood pressure and brain system dysfunction, are divided into three types. Plateau wave or A wave is high amplitude lasting 5-20 minutes at more than 50-100 mmHg. B wave has the amplitude of 0-50 mmHg. C wave has the amplitude of 0-20 mmHg (1).

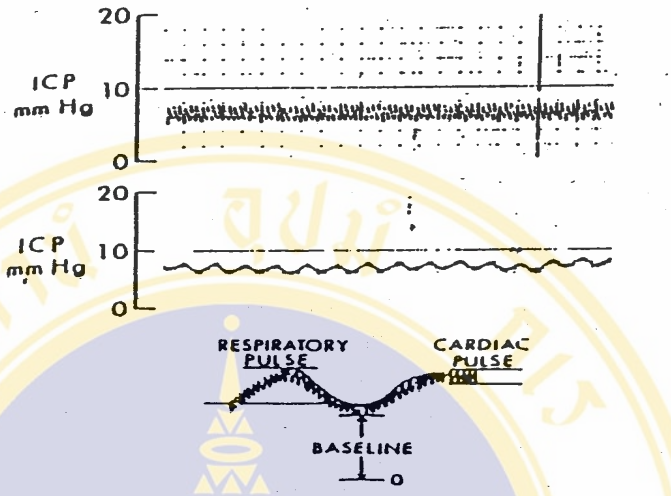

Figure 2.1 Normal ICP wave consisting of baseline, cardiac pulse and respiratory pulse.

2.1.2 Intracranial Pressure Monitoring

Intracranial pressure monitoring can be divided into commercial and uncommercial kits. The commercial kit is a device, which is manufactured by factory or company. These devices consist mainly of the electronic components, which is used to detect the ICP such as epidural or fiberoptic devices. The commercial kit principally consists of a transducer, an amplifier and a recorder. The uncommercial kits use a simple device to measure the ICP such as ventricular catheter and subarachnoid bolt. This device is made from a catheter hose, which has multiple holes to permit better pressure transmission and to reduce the incidence of obstruction (1).

2.1.2.1 Epidural device

The method consists of balloon radiotransmitter of fiberoptic pressure The transmitter is inserted into epidural space as shown in Figure 2.2.

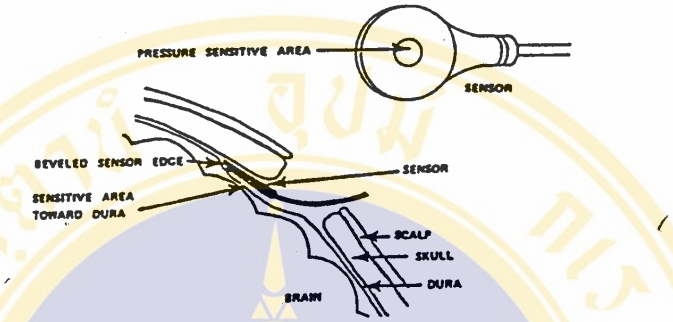

Figure 2.2 Fiberoptic pressure transducer inserted under skull

The advantages of the method are low infection risk and also eliminates risk of intracerebral or subdural hemorrhage. But this method is limited by sensitivity, especially if dura is thick and inelastic, and also inability to drain CSF for ICP control (1).

2.1.2.2 Subarachnoid bolt

This technique uses the catheter that is screwed inside into the subarchnoid and is then connected via a transducer to the monitoring system. This method is easy and does not perforate the skull as shown in Figure 2.3.

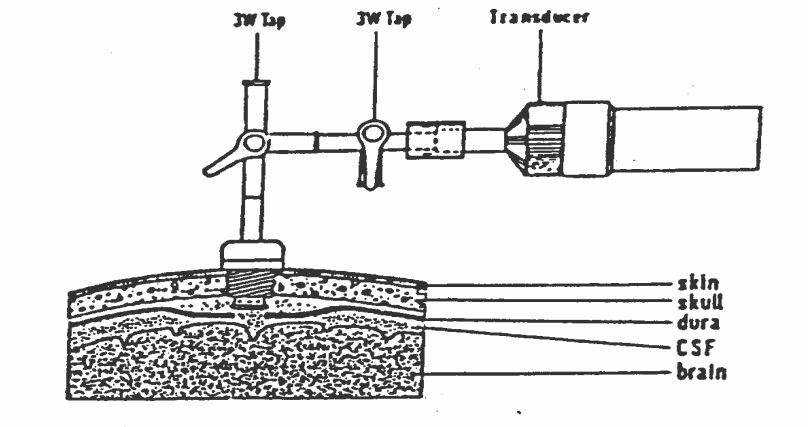

Figure 2.3 Subarachnoid device

The subarachnoid bolt can be used for patients with compressed lateral ventricles and also can be tested for intracranial compliance and reserve, especially low cost (1).

2.1.2.3 Intraventricular catheter

The catheter in this case is inserted into intraventricular in the brain. The catheter is placed on the lateral ventricle position as shown in Figure 2.4

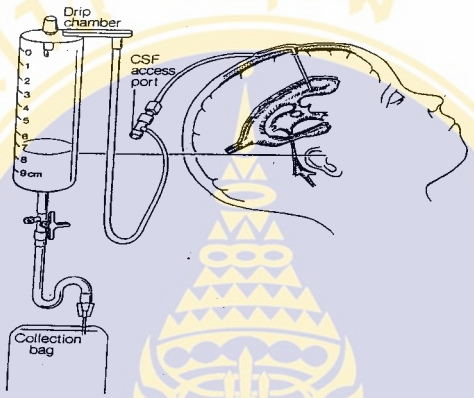

Figure 2.4 Intraventricular ICP monitor with CSF drain system

This method has many advantages: accurate measurement of CSF pressure, ease of sampling CSF for biochemical tests and low cost. Moreover, it can also be used for CSF drainage when necessary. However, infection is the main complication associated with this type of ICP monitoring (1).

2.1.2.4 Intraparenchymal device

This method may be called Camino System, which uses fiber optic pressure transducer connected at the end of the catheter. It can be placed in lateral intraventricular, brain parenchyma subdural or in the brain tissue as shown in Figure 2.5. These methods do not need fluid-coupled, tranducer readjustment and no irrigation. However, the Camino System can not allow CSF drainage and may be broken by bending and twisting (1).

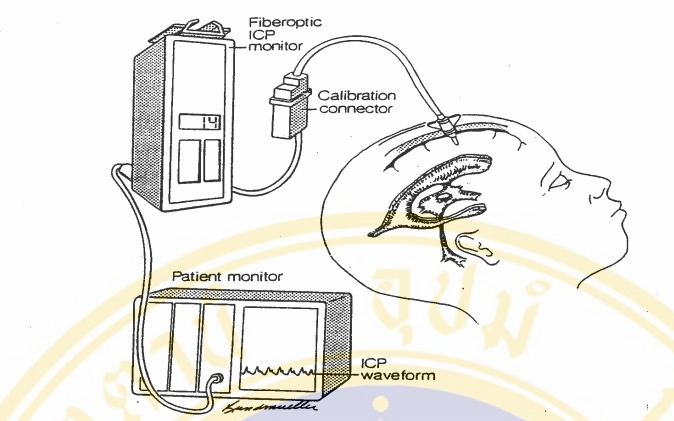

Figure 2.5 Intraparenchymal device and patient monitor

2.1.3 Pressure-Volume Theory

There are three parameters that effect the intracarnial pressure: rate of formation, resistance to absorption and dural sinus pressure. If formation and absorption in balance, there is no alteration in the amount stored, and compartment volume remain unchanged. As long as volume remains constant, pressure remain constant.

When CSF volume is altered, the CSF pressure will change, and amount of pressure change will depend on three factors.

- The rate of volume change
- The amount of volume change
- The intracranial compliance

The change in CSF volume per unit change in CSF pressure defines the intracranial compliance expressed mathematically.

Compliance (C) = change in volume / change in pressure

$$= \frac{\Delta V}{\Delta P} \qquad (2.1)$$

The compliance can also be described as the elastance.

Elastance (E) = change in pressure/change in volume

$$= \frac{\Delta P}{\Delta V} \qquad (2.2)$$

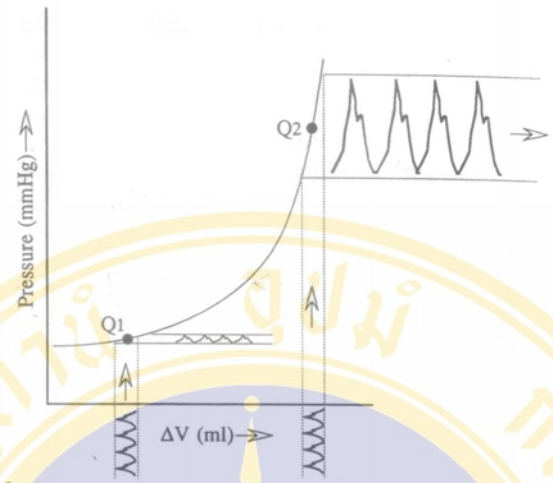

Figure 2.6 Intracranial pressure and CSF volume are exponentially related. Q1 is a equilibrium point on the curve. Volume changes introduced by cardiac and respiratory pulsation are reflected in pressure according at Q1. An increase in pressure shifts the operating point to a new region of curve Q2.

From Figure 2.6, the intracranial pressure and volume are not linearly related, but the relationship changes exponentially with volume. The volume-pressure relationship is described as.

$$P = P_{eq} e^{E1dVe} + P_0 \quad (2.3)$$

where P is ICP, P_{eq} is equilibrium ICP, E_1 is elastic coefficient, Ve is elastic volume and P_0 is a constant term.The exponential variation of pressure with volume is shown in Figure 6. The same volume change on the horizontal axis due to a net intracranial volume perturbation will be reflected as a pulsatile change in pressure, which increases as ICP increases. The exponential curve plots on a logarithmic axis and computing the slope are shown Figure 2.7.

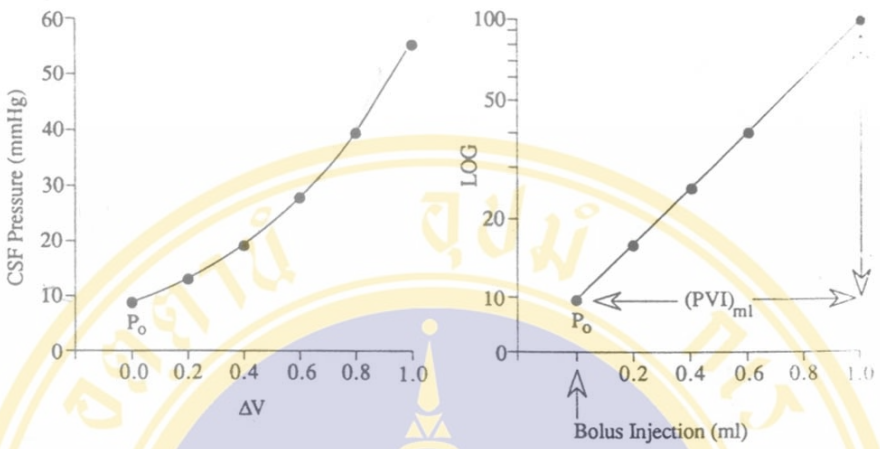

Figure 2.7 The exponential pressure volume curve (left) plotted on a logarithmic axis (right) yields a straight line where the slope of the line is defined as the pressure volume index.

2.2 Electrical volume conductivity

2.2.1 Electrical Conductivity of Tissue

The potential distribution Φ (V) in a volume conductor of tissue is the most important in bioelectric theory. The calculation of Φ is important in impedance measurement, cardiac pacing and defibrillation, electroencephalogram analysis and functional electrical stimulation. The Φ is assumed quasistatic because it often changes slowly in bioelectic problems. Under the quasistatic approximation, the continuity equation states that the divergence, $\nabla\bullet$, of the current dendity, J(A/m^2), is equal to the applied or endogenous source of electrical current, S(A/m^3) :

$$\nabla\bullet J = S \qquad (2.4)$$

Another fundamental property of a volume conductor is that the current density and the electric field, E (V/m), are related linearly by Ohm's Law

$$J = \sigma E \qquad (2.5)$$

where σ is the electrical conductivity (S/m). Finally, the relationship between the electric field and the gradient of the potential (∇) is

$$E = -\nabla\Phi \quad (2.6)$$

If the tissue is an inhomogeneous anisotropy it can be calculated by

$$\nabla\bullet(\sigma\nabla\Phi) = 0 \quad (2.7)$$

Normally, the conductivity is a macroscopic parameter that represents the electrical properties of the tissue averaged in space over many cells. This conductivity is called effective conductivity which consists of real and imaginary parts, and depends on both the temporal and spatial frequencies. The complex conductivity σ* can be described by

$$\sigma^* = \sigma + j\omega\varepsilon \quad (2.8)$$

where ω (rad/s) is the angular frequency and ε is electrical permittivity (S/m). Both the real and imaginary parts of the complex conductivity may depend on frequency. For many bioelectric phenomena, the real part is much large than imaginary part, so the tissue can be represented as purely conductive (8).

2.2.2Resistivity

An electric current can pass through the biological tissues because they have the capability to conducting. This property is characterized by the resistivity, and permittivity. It is independent of the geometry. The resistivity is defined as the real part of the complex valued impedance per unit length and per cross-section area.

The resistivity of a substance can be calculated by using the relationship between electric field (E) and current density (J) distributed in the substance.

$$\rho = \frac{E}{J} \quad (2.9)$$

When, a potential difference (V) is applied between the ends of a wire length L and cross section (A), establishing a current (I) as shown in figure

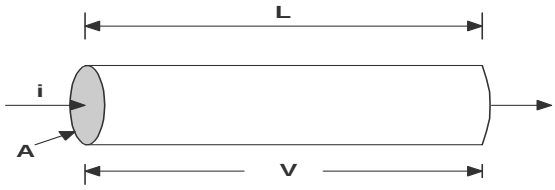

Figure 2.8 Calculation of the resistivity of a substance.

$$E = \frac{V}{L} \tag{2.10}$$

$$J = \frac{i}{A} \tag{2.11}$$

So, we can combine Eq.9, Eq.2.10 and Eq.2.11, we get

$$\rho = \frac{V}{i}\frac{A}{L} \tag{2.12}$$

$$\rho = \frac{RA}{L} \tag{2.13}$$

In medical field, researchers use resistivity of each tissue to study the properties of bioelectric phenomena. The four-electrode method has been used to measure tissue resistivity and impedance (9),(10),(11),(12). Turngikusolmum *et al* applied a four-electrode probe to measure myocardial resistivity of eight open-chest pigs in-vivo at eight frequencies ranging from 1 hz - 1Mhz. They also described the error sources associated with the four-electrode method tissue resistivity measurement.

2.3 Finite Element Method

The finite element method (FEM) is a computer-based method widely used in engineering to solve a variety of problems in structural analysis, heat transfer, fluid mechanics, and other areas. Finite element methods were first introduced in the late 50's and early 60's to solve structural analysis problems in the aerospace industry. Since then the method has grown in popularity and power, to a point where, today, it is used in every day design and analysis in various applications. It can solve problems in heat transfer, fluid mechanics, acoustics, electromagnetic and other specialized disciplines.

The finite element method is a numerical method for solving a system of governing equations over the domain of a continuous physical system. The method applies to many fields of science and engineering. General procedure in finite element method can explain in following steps.

Step 1: Create and discretize the solution domain into a number of elements; that is subdividing the problem into nodes and elements.

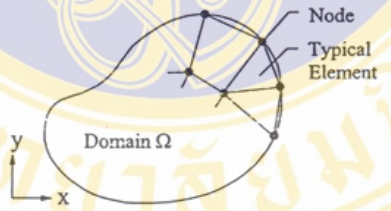

Figure 2.9 Creation the elements.

Step 2: Select element interpolation functions to represent the physical behavior. For example, triangular element consists of three nodes as 1, 2, 3 and three nodal unknowns as ϕ_1, ϕ_2, ϕ_3.

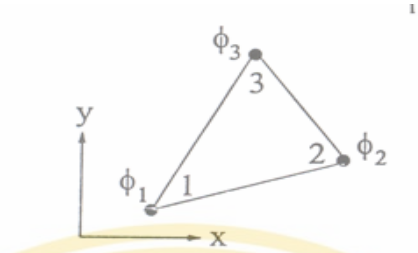

Figure 2.10 Element interpolation functions.

These unknowns may be represented as temperature if we solve the thermal problem. Distribution of element variable is expressed in terms of nodal unknowns as,

$$\phi(x, y) = N_1(x, y)\phi_1 + N_2(x, y)\phi_2 + N_3(x, y)\phi_3 \quad (2.14)$$

where $N_i(x, y)$, I = 1, 2, 3 are the element interpolation function.

$$\phi(x,y) = \lfloor N_1 \quad N_2 \quad N_3 \rfloor \begin{Bmatrix} \phi_1 \\ \phi_2 \\ \phi_3 \end{Bmatrix} = \underset{(1\times3)}{\lfloor N \rfloor} \underset{(3\times1)}{\{\phi\}} \quad (2.15)$$

Where $\lfloor N \rfloor$ is element interpolation function matrix and $\{\phi\}$ is vector element nodal unknowns.

Step3: Set up element equation for each element. For example, the triangular element can be written in matrix form.

$$\begin{bmatrix} k_{11} & k_{12} & k_{13} \\ k_{21} & k_{22} & k_{23} \\ k_{31} & k_{32} & k_{33} \end{bmatrix}_e \begin{Bmatrix} \phi_1 \\ \phi_2 \\ \phi_3 \end{Bmatrix}_e = \begin{Bmatrix} F_1 \\ F_2 \\ F_3 \end{Bmatrix}_e \quad (2.16)$$

Or,

$$[K]_e \{\phi\}_e = \{F\}_e \quad (2.17)$$

This step is very important for finite element equation construction. There are three methods to construct the element equations:

- Direct approach
- Variational approach
- Method of weighted residuals

Step 4: Assemble all element equations to obtain system of simultaneous equation.

$$\sum(\text{Element equations}) \Rightarrow [K]_{sys} \{\phi\}_{sys} = \{F\}_{sys}$$

Step 5: Apply boundary conditions into Step4 and solve for nodal unknowns $\{\phi\}_{sys}$. The nodal unknowns may be displacement, temperatures, flow velocities and other.
Step 6: Compute any other quantities of interest such as the displacements.

2.4 Review of Related work

In brain study, the finite element can be applied to biomechanics and bioelectrical properties study of brain. The primary objective of studying head injury biomechanic is to determine response of brain under various dynamic loading conditions with include transient stress distribution in the brain tissue (13).

For bioelectric properties of brain studies, it involves current density distribution and electric field distribution in brain. These studies, aims are to investigate the biological effects cause by electromagnetic wave from natural and man-made radio source (14), and to predict the current density distribution for measurement or stimulation of bioelectric signal of brain (15).

The validity and efficiency of the finite element technique have been determined and published by many authors. Meanwhile, several FE programs have been particularly developed in order to get the best prediction. It is impossible to exhibit all the applications of FEA in the bioeletric analysis and, therefore, a partial list of published work is given below, many of which involve comparison with experimental results.

Ernest L. Carter *et al* (16) showed that the electrical field and current density distribution were found in the various tissue of a mathematical model of the experimental rat used to study systemic osteoporosis. The finite element method was to solve the boundary value problem derived form Maxwell's equations using a quasistatic approximation for a 60 kHz external output signal applied via skin electrodes. This study was done initially to determine the principle factors, which effect the solution of the field in the vertebral bodies. Grid coarseness, model length, and intervertebral space width had little effect on the solution while trabecular bone and abdominal cavity conductivity values has strong effects. The two pair of transversely placed electrodes spaced by at least three vertebral bodies produced the most uniform field distributions and was used in the experimental rat model. The

range of current density values in the trabecular bone was determined to be 3.0-5.0 $\mu A/cm^2$ at the external output signal where evidence of a reversal of bone loss due to castration osteoporosis had been found in the experimental rat. Moreover, They also applied the FEM to predicted an electrical voltage and current density value for human systemic osteoporosis (17).

Paul Ducheyne *el al* (18) also used a finite element to calculate the electric field gradients and current density present in a rat tibia modeled with a porous intramedullary implant when capacitiverly stimulated. The Maxwell's equations were used to analyse all electrical or magnetic field.

Kamal P.Kothiyal *el al* (19) showed that a finite element analysis technique is used to calculate energy and current density distributions in employed electrode configurations during automatically internal defibrillator. This research determines optimal strategies for these shock deliveries by studying a three-dimensional computer model of the electric fields produced by internal defibrillation electrode.

Marc A. Camacho *et al* (20)also used a finite element to analysis transthoracic defibrillation. They constructed the model of the human thorax is based on a series of cross-sectional CT scans and incorporates isotropic conductivity of skeletal muscle. Current density distribution were determined by Maxwell's equations with two boundary conditions (Dirichiet and Neumann) and compared for four paddle pairs and two paddle sizes.

Weiping Wang and Solomon R. Eisenberg (21) develop a finite element method for determining the spatial distributions of electric fields and current densities in three-dimensional, inhomogeneous, anisotropic nonuniform time-varying magnetic fields. They present a finite element solution method that can be used to compute the induced electric field ad current density distributions in tissue

Kacarska M. *et al* (14) showed that the current density distribution and specific absorption rate (SAR) can be calculated and visualized. To find out position of high energy deposition in brain, they performed finite element simulation for a heterogeneous model of the human head exposed to a linearly polarized RF magnetic field at 900 Mhz. Atsuo Chiba and Kaisul Isaka (22) applied the finite element to the analysis of the current density distribution of the head part composed of scalp, skull, cerebrospinal fluid and brain tissue.

CHAPTER III
METHODS &MATERIALS

3.1 Methodology

The method of this study can be summarized in Figure 3.1. The hypothesis of this study is a changed volume in a brain will effect the electrical conductivity. So, the computer simulation was performed to find the current density distribution on the patient brain model with edema lesion. The simulation is based on the finite element method (FEM), which can be applied to analyze the electrical conductivity of the brain pathology. The bioelectric impedance measurement system was constructed to verify the simulated results of finite element analysis in the consistency check section.

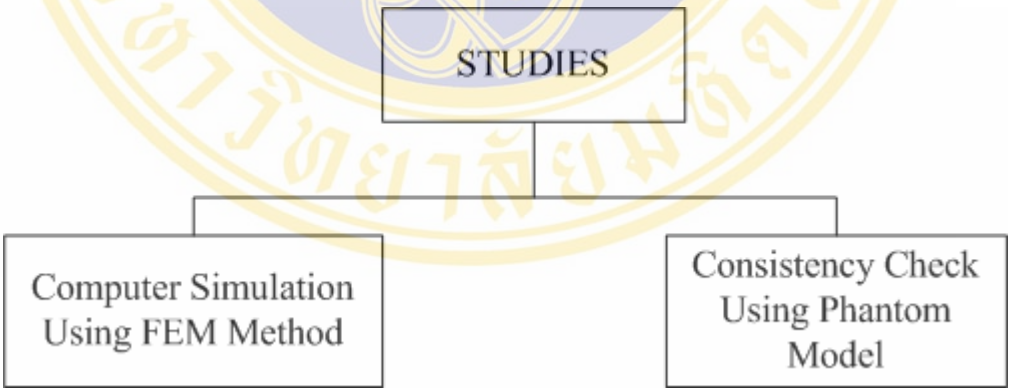

Figure 3.1 Summary of the study

3.2. Computer Simulation

This study is used to predict the current density distribution on the patient brain model with edema lesion. The study is based on an assumption that a variation of fluid's volume will affect the conductivity of tissue. The finite element method is used in this study. The study process is illustrated in Figure 3.2 which is divided into two parts : model preparation and finite element analysis.

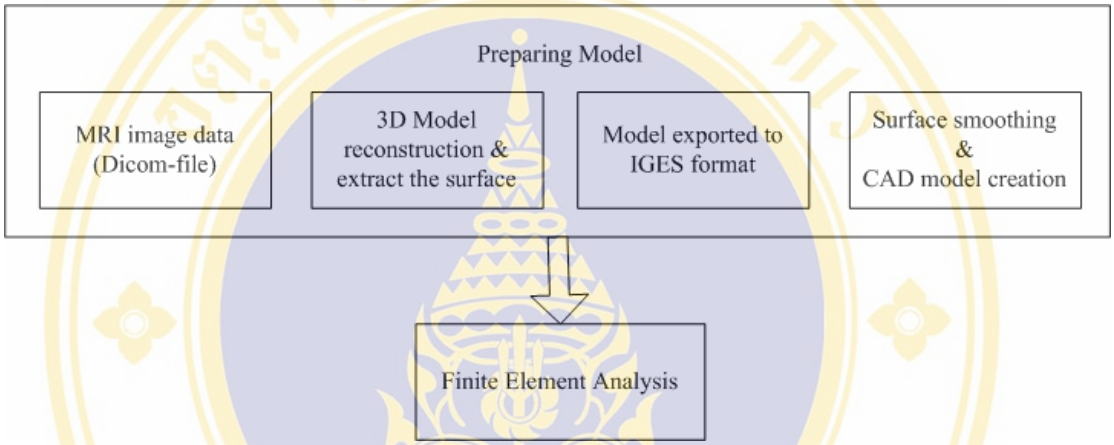

Figure 3.2 The block diagram of finite element study

3.2.1 Preparing 3D Model of Human Head

This process prepares the 3D geometric model for finite element analysis. There are four steps: MRI image data scan, 3D model reconstruction and surface extraction, model exporting and surface smoothing and CAD model creation.

The brain model with edema swelling was created from 75 slices of magnetic resonance images (MRI) with resolution of 256×256 pixel and 0.78 pixel size. The MRI images were taken from a patient with edema condition and stored in the DICOM file format from Siriraj Hospital. The image thresholding was used to extract the surface of different tissue's layers of each slice. There are three layers considered in this study: brain, CSF, skin, and skull. Then, the image data from the thresholding processes was used to reconstruct the 3D model by image processing software (Mimic). Those contours were exported to IGES format, which is displayed in point clouds.

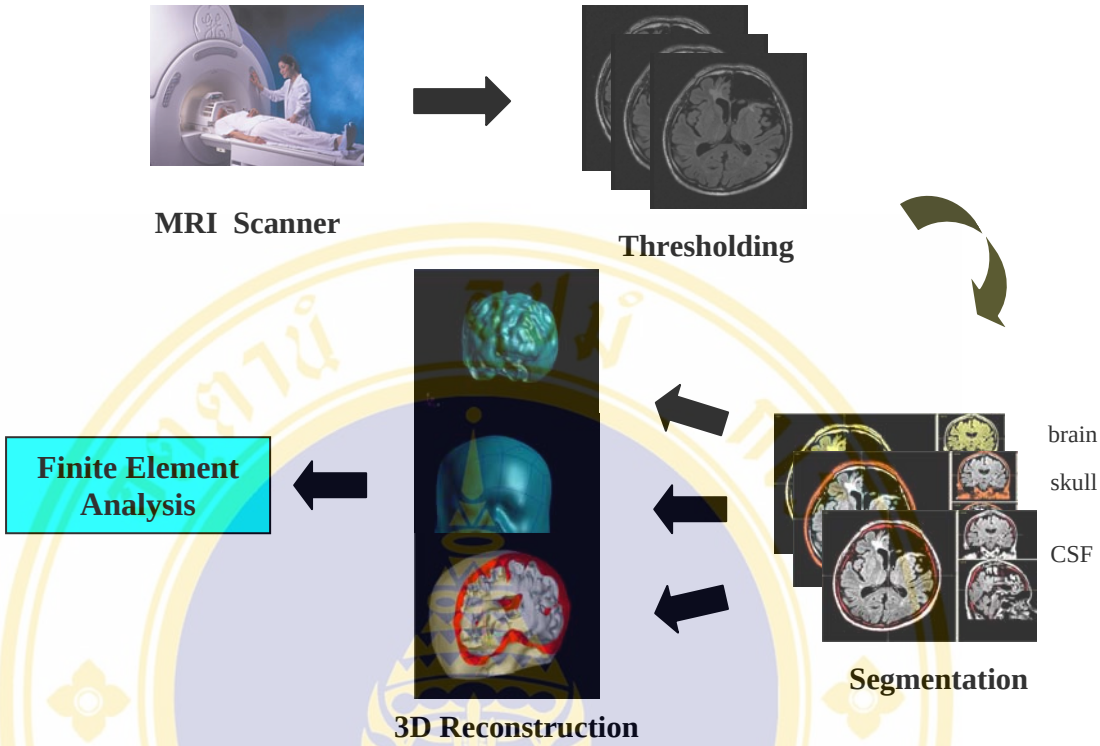

Figure 3.3 Brain model generation procedures

It can be seen from Fig. 3.4 (a) that the surface of the constructed 3D model was not smooth due to image noises and the selected choice of image reconstruction algorithm. The 3D model was later smoothed as shown in Fig 3.4 (b).

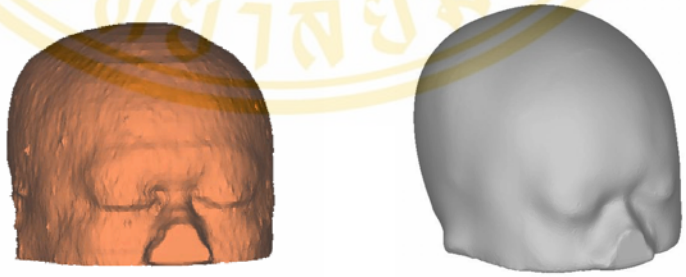

(A) (B)

Figure 3.4 Mesh generation of 3D model: (A) Reconstructed model from MRI images, (B) Smoothed model.

3.2.2 Finite Element Modeling and Analysis

This section can be divided in five parts: mesh and element generation, electrode location assignment, measurement setup, tissue property definition and analysis.

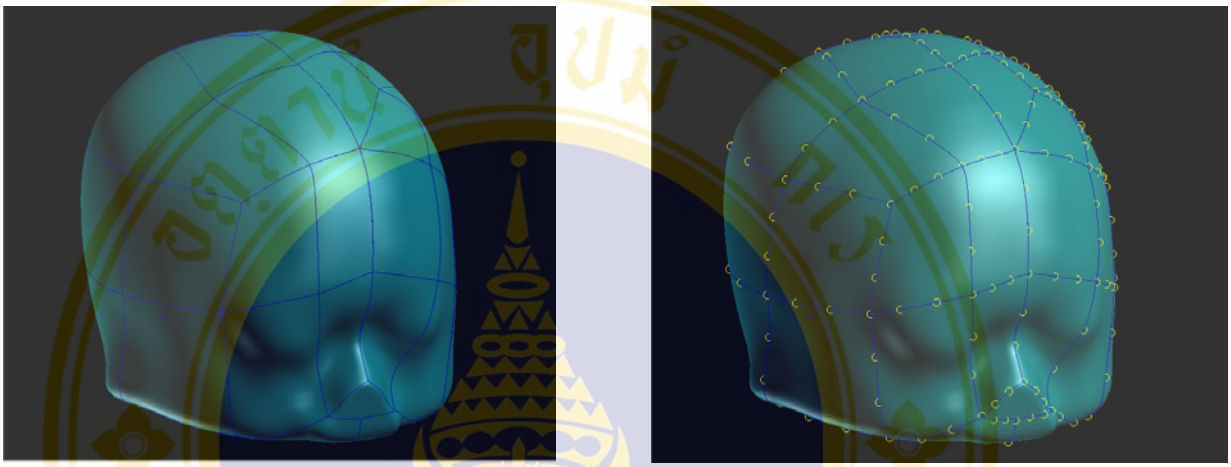

(A) (B)

Figure 3.5 (A) The surface model with wire frame, (B) The seed points were created on the model surface called mesh-seed (yellow points)

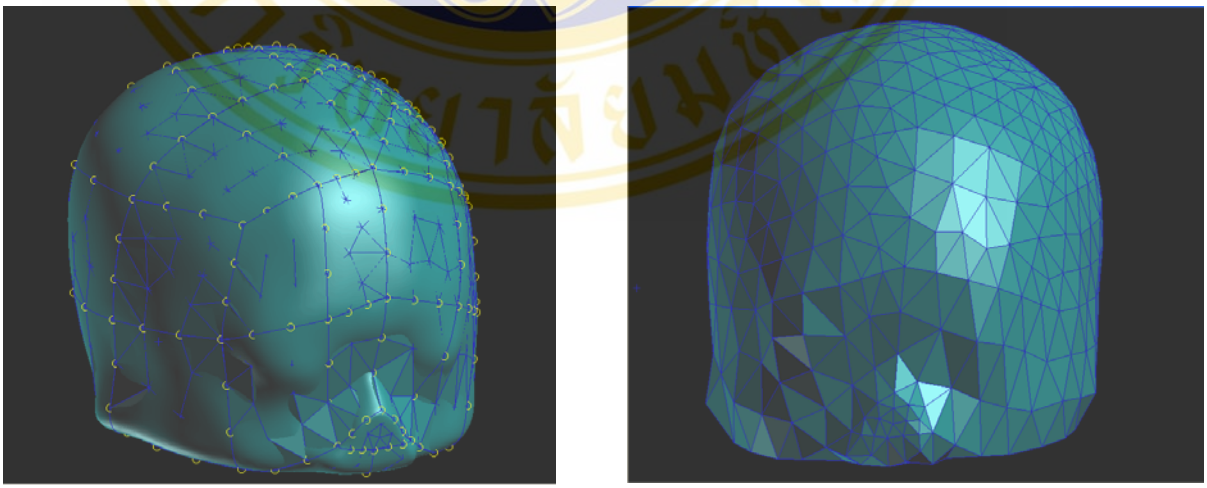

(A) (B)

Figure 3.6 (A) triangular surface meshes model was created on the surface model (B) A triangular element 3D model after finished.

3.2.2.1 Finite Element Modeling

In the previous part, the 3D model (CAD model) was completely prepared. The next step is to apply the finite element method. The 3D models can be used in finite element method as classical mechanic model or CAD model. Some CAD model cannot be used for analysis because the model is not a clean model. Therefore, the model preparation before FEA is an important for analysis. This section illustrates how to obtain 3D CAD model for finite element analysis. The mesh and element creation were perform in five steps using MSC Patran software package. Firstly, the seed points were created on the model surface called mesh-seed generation. The length of seed points were created based on the number of elements on the wire frame. For the element size, an overall element edge length of 3 elements on each wire frame was easily created in a small wire frame.

Secondly, the three –node triangular surface meshes model was performed the node equivalent processes in order to ensure that the surface model generation was entirely enclosed by the triangular mesh without any mesh discontinuities at common face edge. To accomplish this, non- coinciding edge nodes that are closer to each other than a user-defined tolerance value (0.01 mm) were automatically merged together.

Thirdly, the surface meshes have to pass the following test: boundary, duplication, and normal direction of element (all triangular elements must be aligned, meaning that its normal vectors must all point inwards or outwards).

Finally, the three-node triangular surface model was converted into 4-node tetrahedral meshes for each solid based on the triangular surface meshes of its faces.

3.2.2.2 Electrode Location Assignment

In this section, the skull location was assigned by using the 10-20 system given by International Federation of EEG Societies. The locations are used to reference the position on the skull for the analysis. The 10-20 system is used for the EEG measurement. This system is widely accepted to reference the location on the skull. Oostendorp *et al* used this system for conductivity measurement of the human skull (25).

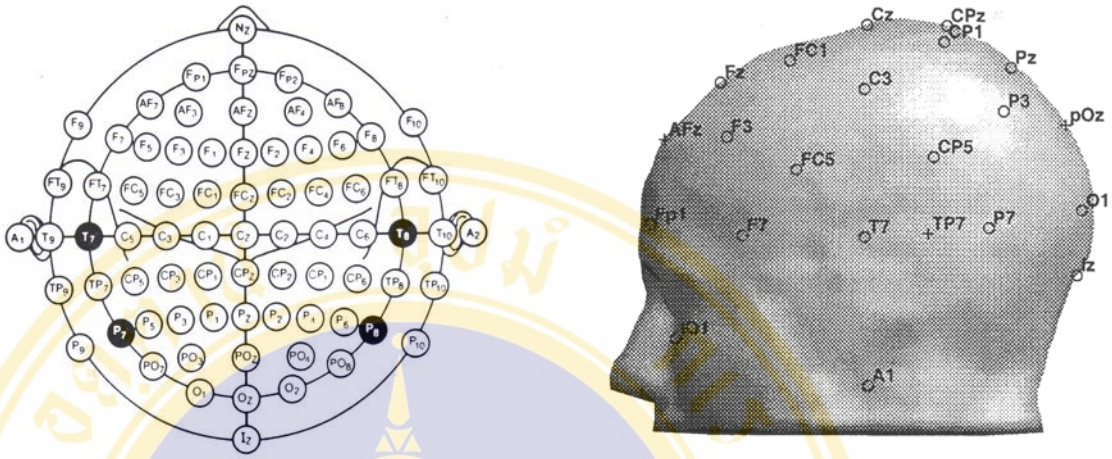

(A) (B)

Figure 3.7 Electrode location: (A) The 10-20 system for EEG measurement, (B) The electrode location on the model.

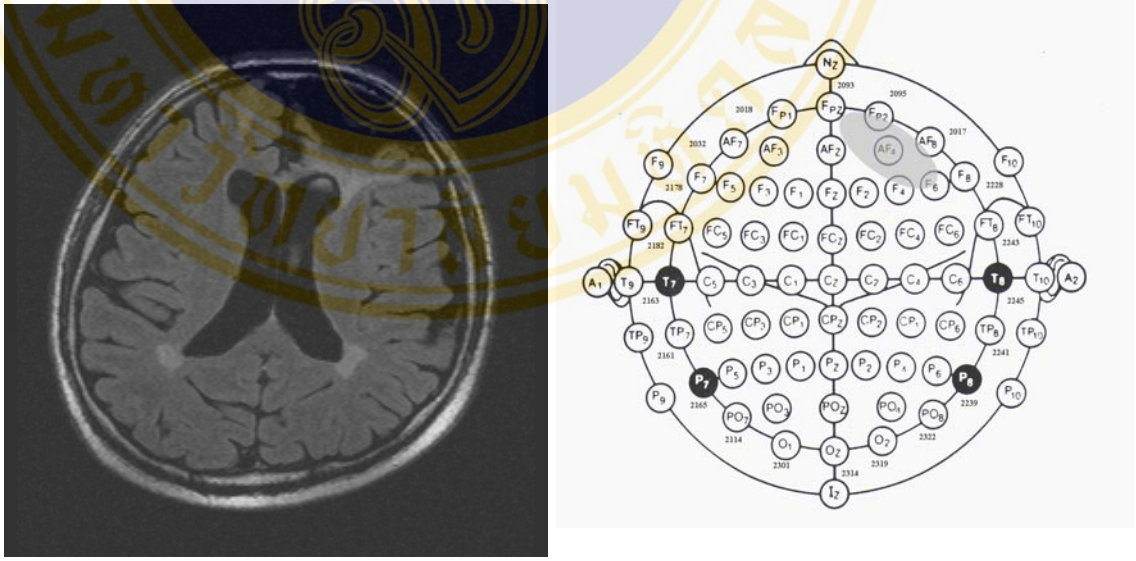

(A) (B)

Figure 3.8 (A) 2D MRI with edema on the frontal lobe of right cerebral hemisphere, (B) The edema location on the 10-20 systems

3.2.2.3 Measurements Setup

The potential distribution on the scalp is generated by applying a constant current through a pair of selected electrodes and then measuring potential on other electrodes. In this work, only electrodes with numbers 2XXX (as shown in Fig. 3.8 (B)) were studied in order to simplify the problem. It is also further assumed that each electrode location is a surface node of the 3D-mesh model.

In brief, the simulation proceeded this way. Firstly, four pairs of electrode locations (Fpz–Oz, T8–T7, F8–P7 and P8–F7) were chosen as shown in Table 3.1. These pairs of electrode locations were used for charge applying locations. A charge of 1 mC was assigned to the charge applying electrodes (once chosen). Then, for each charge applying location pair, potential values were measured according to locations given in the left column of Table 3.1.

Table3.1 Electrode locations for applying electric charges and measuring potential values.

Charge Applying Locations	**Potential Measuring Locations**
FPz - Oz	FP_2 AF_8 F_8 FT_8 T_8 TP_8 P_8 PO_8 O_2 FP_1 AF_7 F_7 FT_7 T_7 TP_7 P_7 PO_7 O_1
T8 - T7	FT_8 F_8 AF_8 FP_2 FPz FP_1 AF_7 F_7 FT_7 TP_8 P_8 PO_8 O_2 Oz O_1 PO_7 P_7 TP_7
F8 - P7	AF_8 FP_2 FPz FP_1 AF_7 F_7 FT_7 T_7 TP_7 F_8 FT_8 T_8 TP_8 P_8 PO_8 O_2 Oz O_1 PO_7
F7 - P8	TP_8 T_8 FT_8 F_8 AF_8 FP_2 FPz FP_1 AF_7 PO_8 O_2 Oz O_1 PO_7 P_7 TP_7 T_7 FT_7

3.2.2.4 Tissue Property Definition

The tissue properties (skull, CSF, Brain) were defined. Tissue conductivity was assigned to all 3 regions of the model. The conductivity of tissues in human brain is highly anisotropic and heterogeneous that are more complex (4). In this study, we assumed that the brain is isotropic, homogeneous and quasi-static (6). The isotropic properties assumption means that the material properties do not depend on the orientation of field vectors. The homogeneous assumption means that material property values remain constant throughout the volume. The conductivity values used in this study was taken from literature (6) as shown Table 3.2.

Table 3.2 The tissue properties of each layers for brain model

Tissue	Conductivity (S/m)
Brain	0.25
CSF	1.75
Skull	0.018

3.2.2.5 Finite Element Analysis

In our study, the electrostatic analysis approach was used to compute electric field (E) and electric displacement flux density (D) using the following Maxwell's equations.

$$\nabla \cdot D = \rho \quad \text{and} \quad \nabla \times E = 0 \tag{3.1}$$

$$D = \varepsilon E \quad \text{and} \quad E = -\nabla\phi \tag{3.2}$$

where ε is electrical permittivity (F/m), D is electric flux density (C/m^2), E is electric field (V/m), and ϕ is electric potential (V). The electric flux density in dielectric materials and current density in conducting materials are an analogy between one and another because electric flux density and current density are linearly related to the electric field. Thus, we can derive electrostatic equation in conducting materials assuming that the displacement current, D, is zero. Due to the fact that we are doing electrostatic analysis, the divergence of current density, J, equals zero

$$\nabla \cdot J = 0 \quad \text{and} \quad J = \sigma E \tag{3.3}$$

$$\nabla \cdot [\sigma \nabla \phi] = 0 \tag{3.4}$$

where σ is electrical conductivity (S/m), and J is current density (A/m^2). There are two boundary conditions for finite element analysis (7,8). The first boundary condition requires that there is a constant charge applied to node on the brain model (Dirichlet boundary condition). The second boundary condition specifies that the normal derivatives of the potentials are zero at boundary points on the model's surface (Neumann boundary condition)

3.3 Consistency Check

Normally, the accuracy of the FEA prediction is dependent upon how accurate the material data and environmental boundary condition are defined. In many applications, precise material data are difficult to determine experimentally. Especially, the brain conductivity values provided by many researchers are different for example conductivity value, temperature, frequency, and injected current.

This section was provided to check the FEA results that have a consistent value to experimental results. Generally, the result obtained from analysis is an approximation. However, result can represent behavior of the electrical distribution in the brain. Moreover, the conductivity of human skull is lower than the scalp and brain which is a major problem for electrical impedance measurement. The more resistivity of the skull will decrease the sensitivity of the impedance measurement. So, a checking system was design in this section to confirm the result and those behaviors that can be detected by using electrical impedance measurement. This section consists of three steps: electrical impedance design, preparing tissue-equivalent phantom, experimental setup and experimental procedure.

3.3.1 Electrical Impedance Measurement System Design

The checking bases on the bioelectric impedance measurement. Figure 3.9 illustrated the system block diagram. The system operation is controlled by PIC

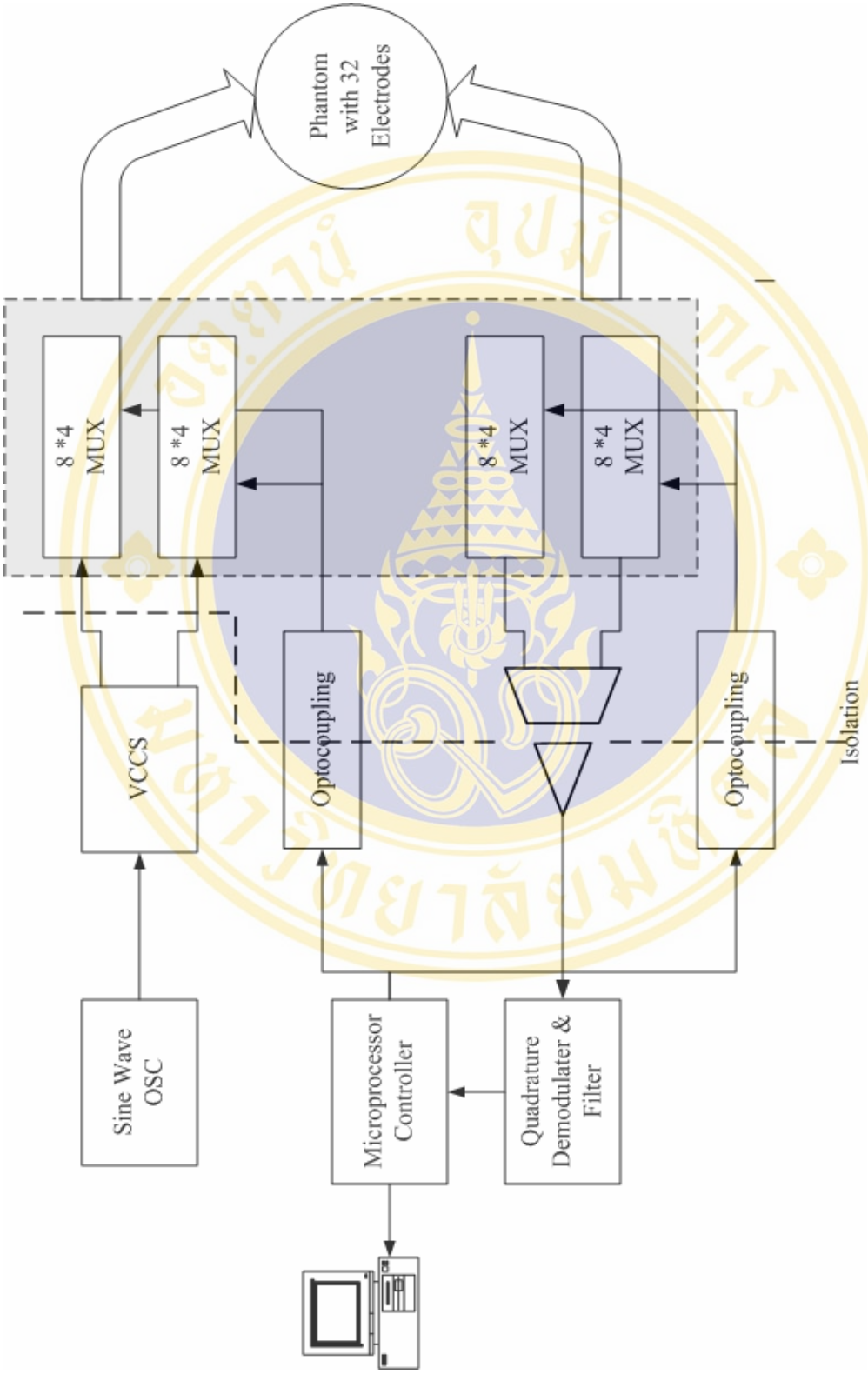

Figure 3.9 The system block diagram of electrical impedance measurement system

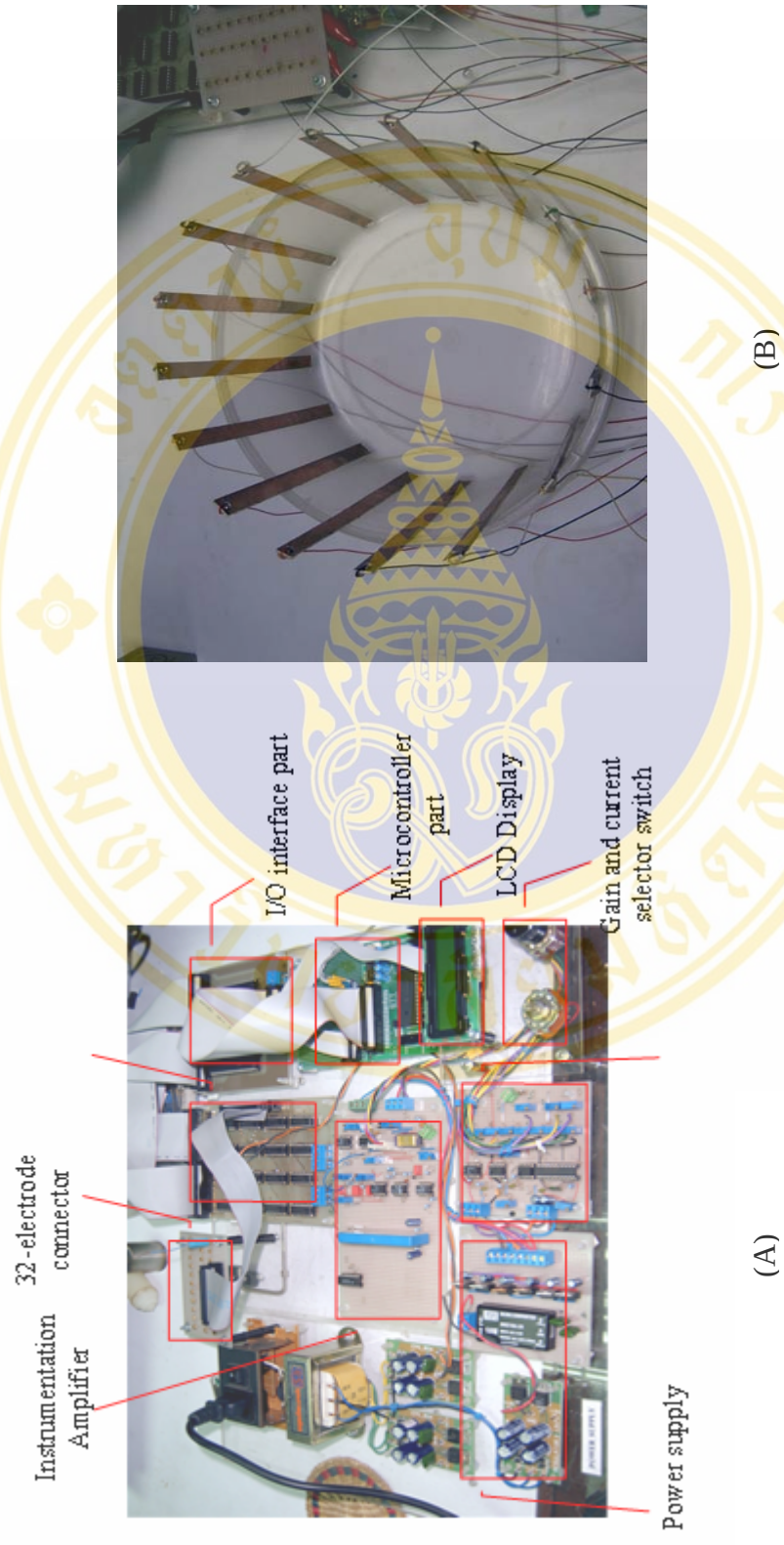

Figure 3.10 (A) Prototype system of the electrical impedance instrument, (B) Cylindrical-shape phantom with strip electrodes

18F458 microcontroller. This system consists of eight parts: sine wave oscillator, voltage-to-current converter (V/I), multiplexer (MUX), 32-electrodes, digital coupler, amplifier, demodulator, and microcontroller. The basic operation of each part was described in Appendix A. PIC-Basic program was used. Figure 3.11 shows the flowchart of the control program in the microcontroller.

3.3.2 Tissue-equivalent Material Preparation

Saline with known concentration was used to prepare the tissue-equivalent materials. A tissue-equivalent material means that it must have the equivalence of electrical conductivity property (to the actual tissue in human body). The saline was prepared from sodium chloride and deionization water. There are three saline conductivities which were prepared as shown in Appendix B. These tissue-equivalent's conductivity were measured 1.42×10^{-3}, 6.25×10^{-3} and 4.34×10^{-3} Ω/cm, respectively. The concentration of saline were 0.0276 molar at 680 ml, 0.034 molar at 920 ml, 0.159 molar at 628 ml for white mater, blood and tumour conductivity, respectively. Conductivity meter (Inolap cond level 2, Model Tetracon 326) was employed to confirm measured conductivity value of each saline. Five grams of agar powder was added into saline of 1.42×10^{-3} and 6.25×10^{-3} Ω/cm conductivity. Then, saline with agar powder was cooked to make tissue-equivalent materials (blood and tumour). After the agar setting, they were divided into four sizes: 1 cm^3 ,5 cm^3 ,10 cm^3 ,15 cm^3 and 50 cm^3 as shown in Figure 3.12. All of those processes were done in the chemical lab, department of chemical engineering, Mahidol University.

3.3.3 Experimental Setup

The experimental arrangement for potential distribution measurement is shown in Figure 3.13. A system consists of a cylinderical phantom, electrical impedance instrument, electrode and tissue-equivalent materials. The shell phantom was made from plaster with 18 cm diameter and 1.5 cm thickness. There are two types of electrodes were used in the experiments: strip and point electrodes. Strip electrodes were made of 1 cm wide of long strip copper. Point electrodes were made of Ag/AgCl.

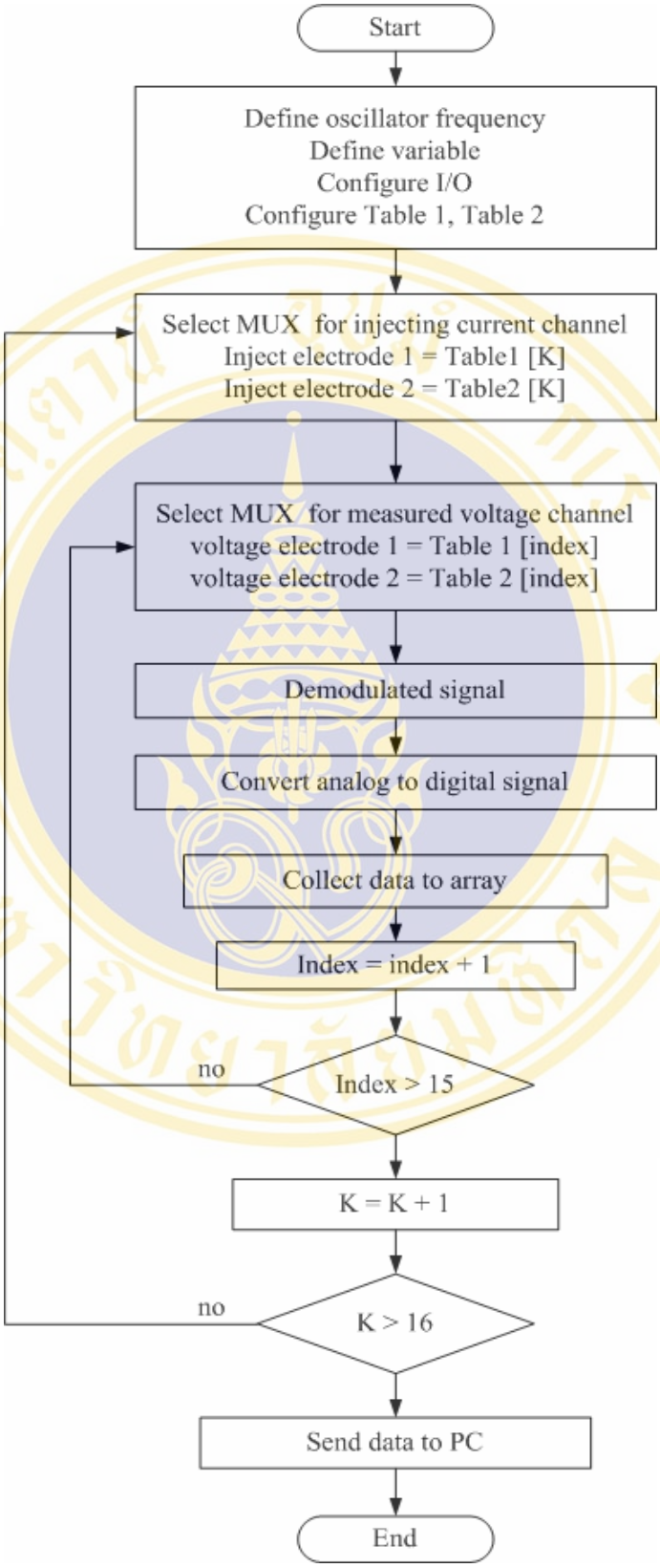

Figure 3.11 A flowchart of the PIC basic program for data acquisition

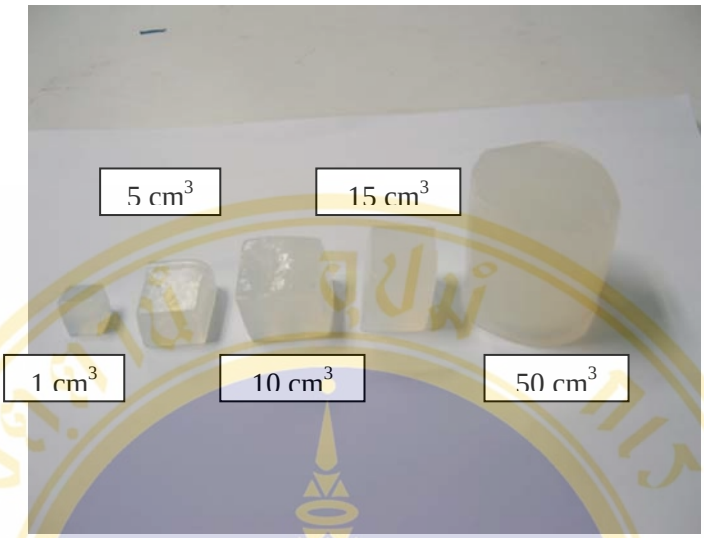

Figure 3.12 Tissue-equivalent materials which represents the edema and tumour lumps.

3.3.4 Experimental procedure

There are three main experiments in this phase. First, the edema situation was simulated in the phantom to investigate whether electrical impedance measurement can detect edema condition.

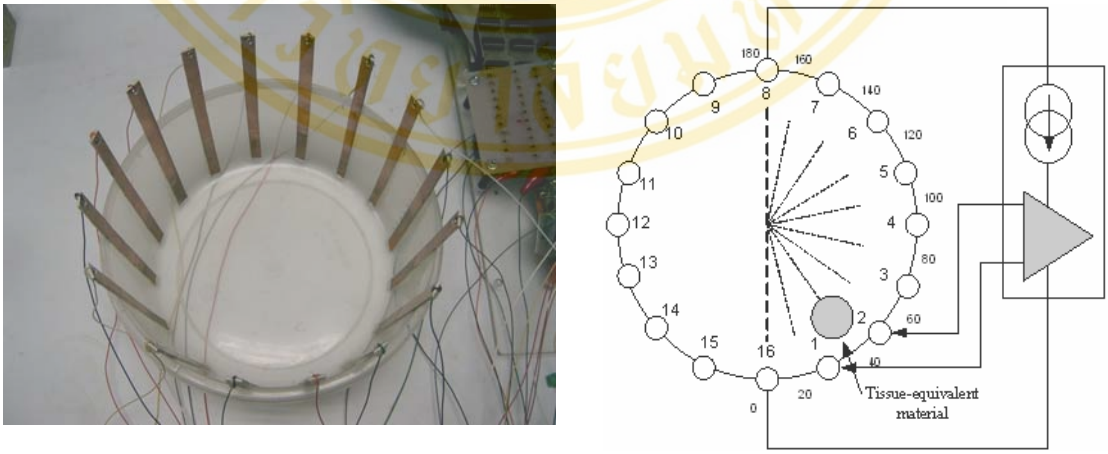

(A) (B)

Figure 3.13 A system used for the first experiment, (A) cylindrical phantom with 16-strip electrodes, (B) A connection of electrical impedance instrument on the phantom.

This experiment was performed to determine the potential distribution on a cylinder phantom with the tissue-equivalent material inside (representing blood and tumour lump). Measurement was performed on a saline conductivity of 1.42×10^{-3} Ω/cm (representing brain white matter) with a level of 3 cm high in the phantom. The 16 strip electrodes were placed around the phantom. Then, a tissue-equivalent material (representing edema lump) is inserted in the phantom at 40 degree location. After that, a constant alternating current was applied through electrodes 8 and 16 (Figure 3.13 B). Then, potential distribution was measured with electrode pairs 1-2, 2-3, 3-4 … 14-15. So, the 12 voltage measurements were obtained from these measurements (one measurement cycle).

The next sets of 12 voltage measurements were obtained by changing the tissue-equivalent material to other locations such as 60, 80, 100, 120 and 140 degrees. These experiments were performed by injecting alternating current of 1 mA at various tissue-equivalent material size (1cm^3 5, cm^3, and 10 cm^3). A data acquisition pattern was defined by a program in the microcontroller which is illustrated in Figure 3.11.

The second experiment was performed to determine the skull effect on the potential distribution. The experiments consist of cylindrical phantom, strip and point electrodes and 10 cm^3 tissue-equivalent material. The skull was simulated by a shell of the phantom made of plaster as shown Figure 3.14 (A). The strip electrodes were placed around the cylindrical plaster phantom and tighten by an elastic belt. Then, the potential measurement procedure was performed the same as the fist experiment.

Finally, after finishing previous experiment, the strip electrodes were changed to point electrodes. The measurement was repeated by using the same procedure.

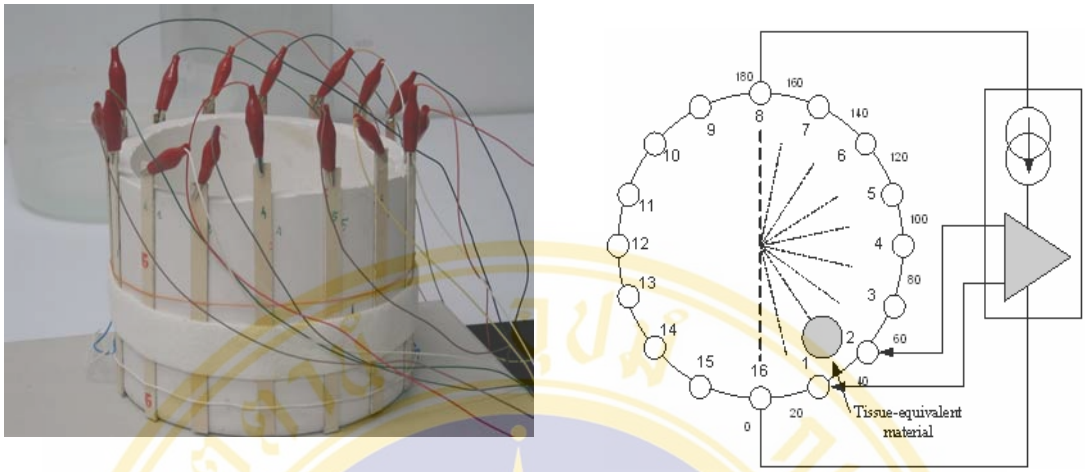

(A) (B)

Figure 3.14 A system used for second experiment, (A) cylindrical plaster phantom with 16-strip electrodes, (B) A connection of electrical impedance instrument on the phantom.

CHAPTER IV

RESULTS

This chapter is divided into two parts. The first part is the simulation result, which covers the finite element prediction. The second part is the consistency check result by using the phantom. The four experiments are performed. Results are shown in this part.

4.1 The Computer Simulation Results

The potential distributions on the 3D finite element model with edema lump were shown in Figure 4.1. Figure 4.1 was plotted between potential distributions and location around 3D model. Red and green lines represent the potential distribution on the right and the left of model, respectively. The lesion of edema was illustrated by black line. Figures 4.1 (A) and (B) showed the electric potential profiles along the electrode locations (shown in Tab. 1), while charge applying electrodes are at P8-F7 and FPz-Oz, respectively. The results showed that the edema lump affects the electrical potential around the models. These results indicate that edema lump causes a difference in potential distribution. The measured potential values in the CSF and brain tissue regions are attenuated more than 85% through the skull (170 mV on the skull layer to 23 mV on the CSF layer). The results confirms previously published findings.

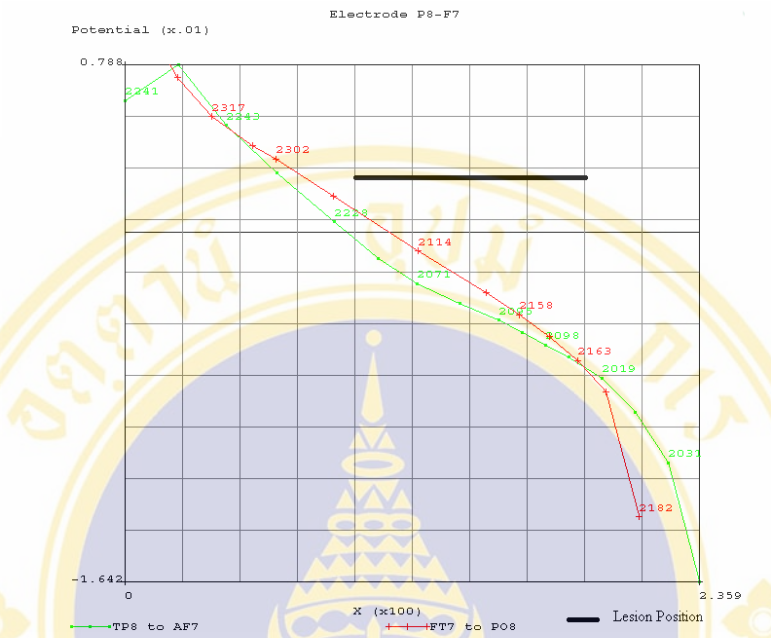

Figure 4.1 (A) Electric potential profile when charge applying electrodes are at F8-P7

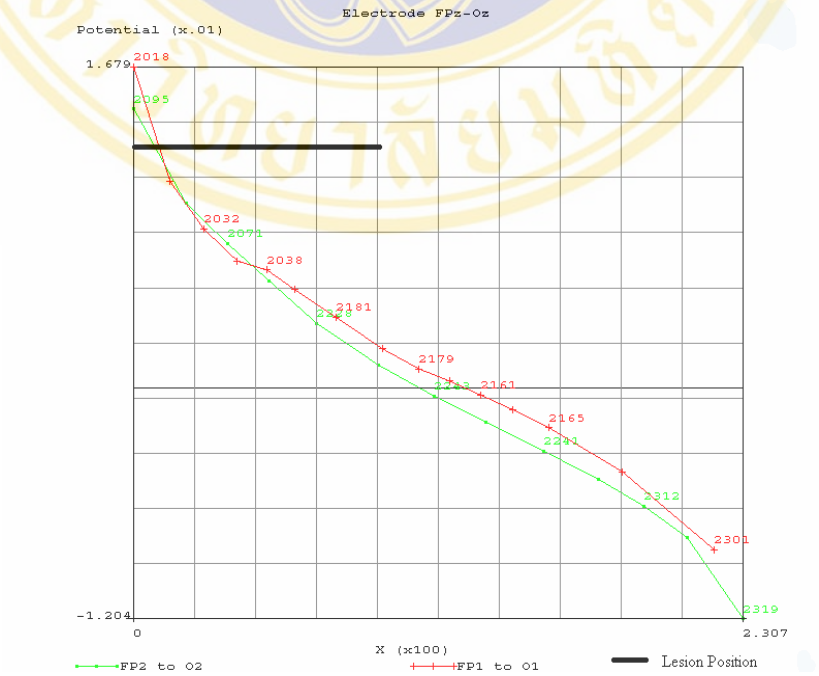

Figure 4.1(B) Electric potential profile when charge applying electrodes are at FPz-Oz

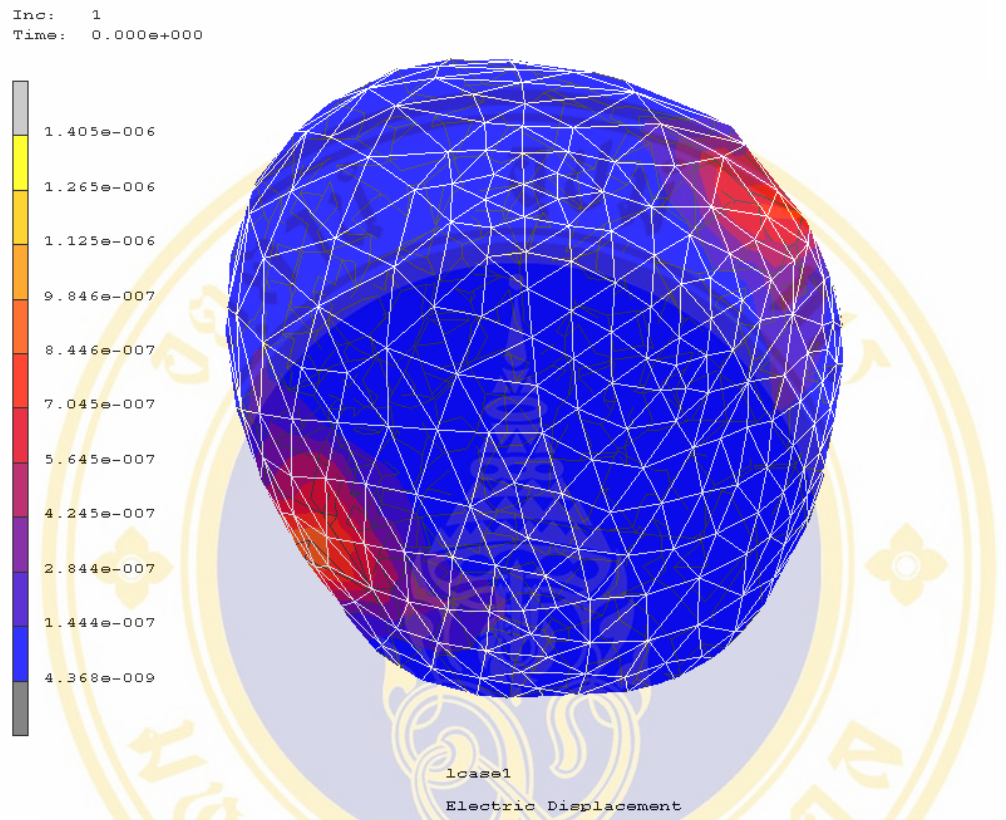

Figure 4.2 Surface electric potential distribution (charge applying electrodes at F8-P7)

The surface electric displacement current on the 3D model was shown in Figure 4.2. Figure 4.2 illustrates when charge-applying electrodes are placed at F8-F7 locations.

4.2 The Consistency Check Result

Figure 4.3 illustrates potential distribution around the phantom model with tissue equivalent materials representing edema and tumour lump. The potential distribution was measured at various angles as shown in Figure 4.3. Note that one pair of electrode is used for constant and fixed frequency alternating current injection. The following results indicate that the potential decreased when the edema lump is located near the measuring electrodes.

Figure 4.3 (A) shows the potential distribution on the phantom model when applied the 1 mA current and inserted the 1 cm^3 edema lump (tissue-equivalent). The results indicate that the voltage will drop from normal level (the voltage level when the edema lump is not inserted in the phantom) when the edema lump located near the measurement electrodes. From this figure, the voltage potential dropped from 1.8 V to 1.6 V when the edema lump is located near the measurement electrodes. A differential voltage obtained by 1 cm^3 edema lump is quiet a small value. The differential voltage was associated with the size when the measurement is performed with 5 cm^3, 10 cm^3 ,and 15 cm^3 of edema sizes as shown in Figure 4.3 (A-D) respectively.

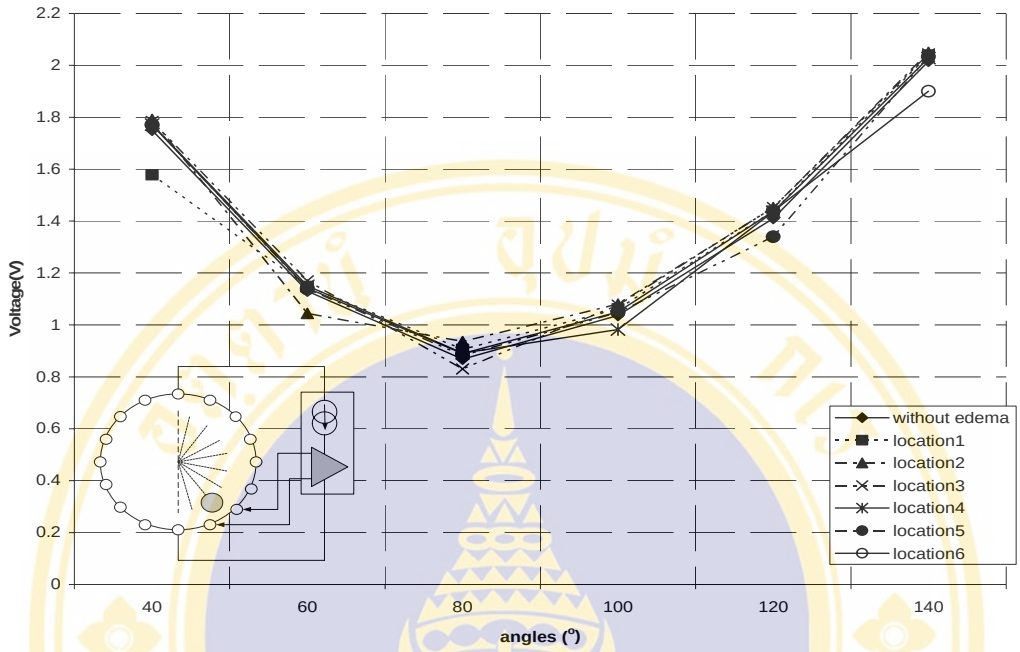

Figure 4.3 (A) The potential distribution on the cylindrical phantom of 1 cm^3 edema lump

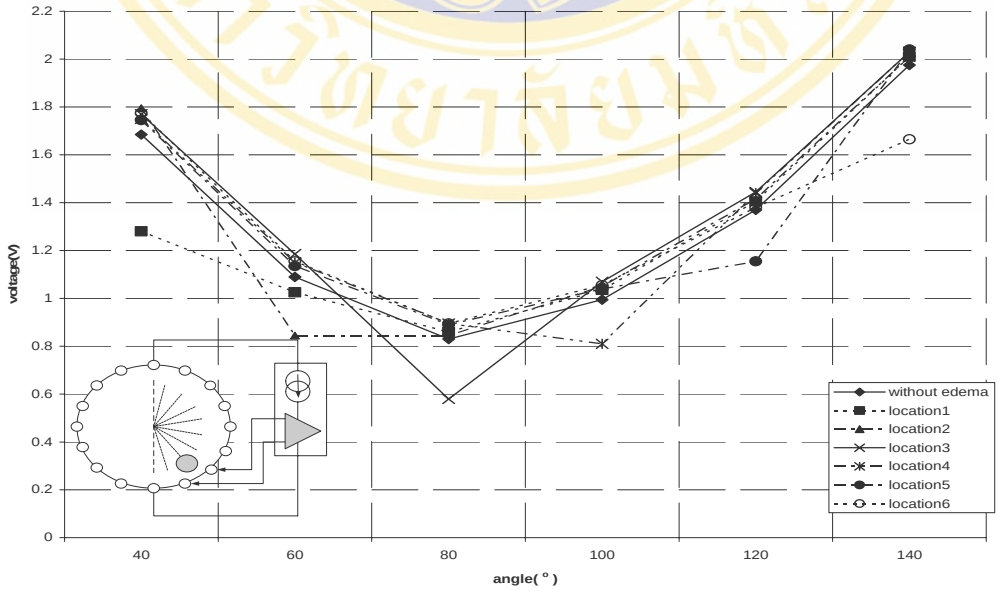

Figure 4.3 (B) The potential distribution on the cylinder phantoms of 5 cm^3 edema lump

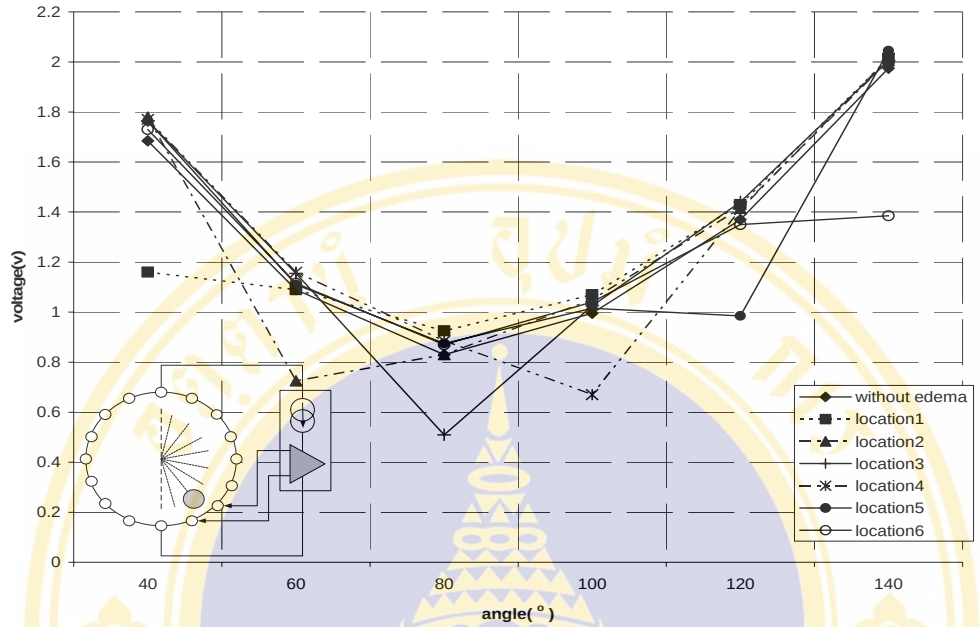

Figure 4.3 (C) The potential distribution on the cylinder phantoms of 10 cm3 edema lump

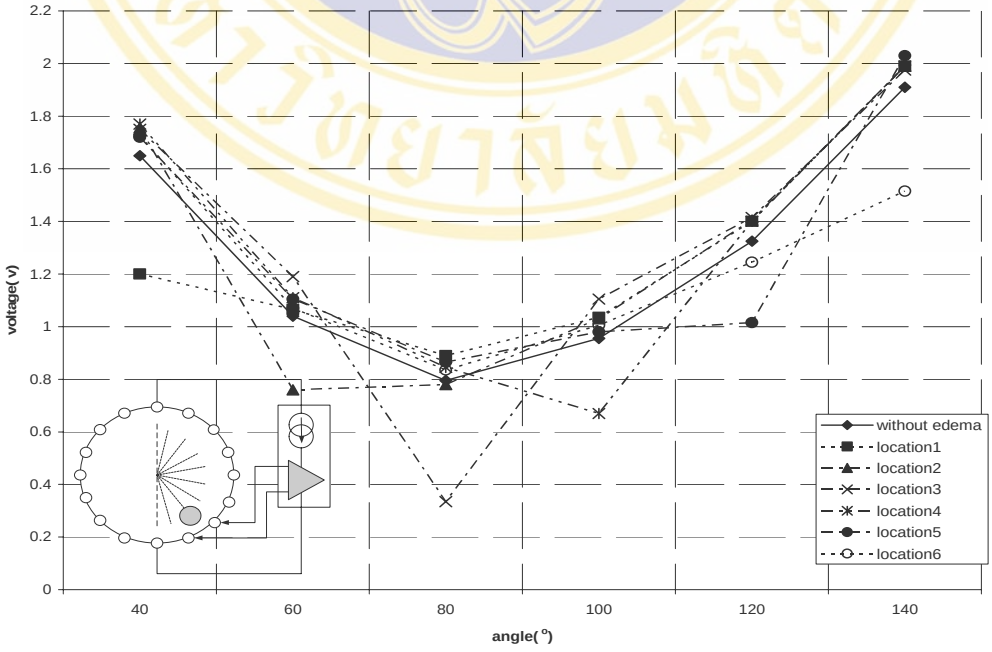

Figure 4.3 (D) The potential distribution on the cylinder phantom of 15 cm^3 edema lump

Table 4.1 The potential distribution of edema and tumour lump on the cylinder phantom with strip electrode measurement.

	Edema lump				Tumour lump			
angle (^{o})	1 cm^3	5 cm^3	10 cm^3	15 cm^3	1 cm^3	5 cm^3	10 cm^3	15 cm^3
40	1.58	1.28	1.20	1.16	1.59	1.44	1.28	1.12
60	1.044	0.845	0.76	0.725	0.985	0.85	0.75	0.61
80	0.83	0.58	0.51	0.335	0.765	0.61	0.51	0.37
100	0.982	0.81	0.67	0.67	0.94	0.78	0.71	0.525
120	1.34	1.155	1.015	0.985	1.3	1.085	1.01	0.875
140	1.9	1.665	1.515	1.385	1.865	1.64	1.54	1.345

Table 4.1 summarizes the potential distribution on the cylindrical phantom when injecting 1mA current with various tissue-equivalent volumes (edema and tumour materials) 1cm^3, 5 cm^3, 10 cm^3, and 15 cm^3. The measurement was performed with varied locations of edema and tumour lump as 40 – 140 degree (20 degree for each step). The results indicate that the potentials at 40 and 140 degree are higher value than other location. The amplitude of those potentials are higher at 40 degree, then slightly decreases and turn to slightly increases, after that it is higher at 140 degree again. The potential distribution amplitude of 15 cm^3 tissue equivalent volume is lower at 40 and 140 degree than other volumes. It appears that the varied potential distribution values are depending on the volume of the tissue equivalent materials. The potential distribution of edema and tumour lump shows the same behavior but different in details.

Table 4.2 The potential distribution of 10 cm^3 edema lump on strip and point electrodes

Angle (^{o})	strip electrode	point electrode
40	1.105	3.958
60	1.055	1.071
80	0.84	0.835
100	0.835	0.563
120	0.975	0.823
140	0.975	3.544

Table 4.2 illustrates the potential distribution of strip and point electrode measurement. The measurement was performed on the plaster cylindrical phantom with 5 mA of injection current. The potential distributions are similar pattern in Figure 4.3 (first experiment). The potential profiles shows the same behavior in both cases but the peak amplitudes are different at 40 and 140 degrees. The potential measured from the point electrodes is higher than strip electrodes at the angle of 40 and 140 degrees. The current injection was higher value than the first experiment. These results imply that a shell of the phantom affects the current distribution of current injecting electrodes.

Table 4.3 potential distribution on the phantom with edema lump size.

size	40^o	60^o	80^o	100^o	120^o	140^o	% difference from normal level
1 cm3	0.172	0.086	0.038	0.054	0.07	0.116	6.3
5 cm3	0.405	0.245	0.25	0.185	0.33	0.31	22.5
10 cm3	0.45	0.28	0.46	0.285	0.31	0.395	31
15 cm3	0.525	0.365	0.32	0.325	0.385	0.59	32.3

Table 4.3 summarizes the results of potential distribution with different volumes (sizes of edema lump). Those potential values were calculated from normal level and dropped potential. The results indicate that the 1 cm^3 edema causes the potential to fall from normal level (6.3 % approximately). A bigger size of edema had a higher different potential than the smaller sizes as can be seen in Table3.3.

CHAPTER V
DISCUSSION

This section discusses the result of finite element analysis and the model validation. The suggestion and recommendations are included in this section.

5.1 Computer Simulation

The results indicate that the electric potential picked up from the region near the lesion location tends to be lower than the area without the lesion. The potential difference due to the asymmetrical distribution is in the range of 100-300 mV, approximately. The implication of this result is that the edema lump effects the electric potential distribution on the model. The reason for different potential distribution is a different conductivity of tissues. Especially, the edema conductivity has a high conductivity (1.75s/m) than other tissues. The different conductivity leads to non uniform equipotential distribution (3). The edema location has a high conductivity than tissues around it. So, the current line will pass through that area, thus, high density of current at the edema lesion. That density causes the equipotential near the edema lesion to be shifted resulting in the decreasing potential distribution at a pairs of measured electrode.

The accuracy of the finite element analysis depends on many factors. The following topic explains some cause that effects the finite element analysis.

- The electrostatic equation was used in FEA which is based on the Poisson's equation. These equations describe the electric fields produced by stationary distribution of electric charges. This is not time varying equation. Actually, human head have the dura membrane which is a tissue membrane cover the brain tissue like a capacitor. However, many researchers have used these equations for electric potential calculation and ignored the capacitive effects. In bioelectric problems, potential distribution often changes slowly which can assumed that it is quasistatic (23). If the time varying equation is used, the simulation is more accurate.

- The 3D-head model was generated from MRI images of a real patient with brain edema. This model is very complex model. For model preparation, some detail was intentionally ignored by thresholding and segmentation processes. Moreover, in order to simplify the model element generation, complex structure in the brain were ignored. Some detail of human model was lost. However, the main structure are still in the brain model, e.g., skin, skull, CSF, brain and edema lump.
- In this study, the model's properties were assumed to be isotropic and homogeneous that means the conductivity of material (tissue: skin, skull, brain, CSF) is the same value in everywhere. In living tissue, such as the brain, especially white matter, the axons are organized into white matter fiber tracts, which are anisotropic. These conditions are not the same conductivity value on vertical and horizontal axials (heterogeneous). However, Pedro C. (22) reported that a homogeneous isotropic modal has an error of about 5% in the region of interest.

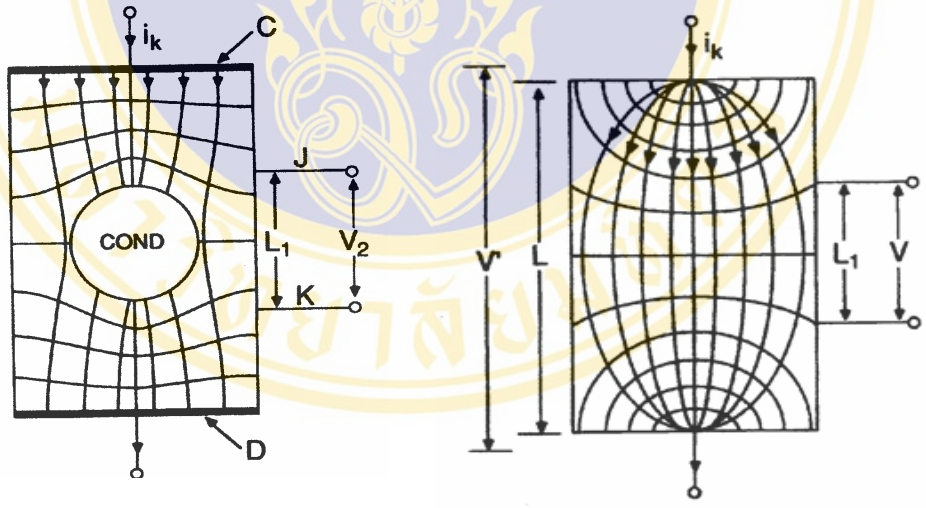

(A) (B)

Figure 5.1 Two-dimensional of current and equipotential line in a rectangular conductivity cell, (A) Effect on the current and potential distribution of inserting a sphere of high conductivity into the conductivity cell with end plate electrodes C and D containing conductor, (B) Current and potential distribution if the current is introduced into the cell using small electrodes.(Baker : 1989)

5.2 Consistency Check

The electrical impedance measurement system was designed and constructed to check the finite element model. From figure 4.3 (A-D), the results show that the edema lump (tissue equivalent materials) causes the decreasing of the potential distribution around the phantom when injecting of 1 mA of alternating current. The current is injected through electrode 16 and 8 as shown in Figure 4.3. This method is called opposites method for measurement impedance. The current distribution in this method is uniform and has a good sensitivity. The potential distributions were highest value at 40 and 140 degrees than other locations because the locations of measurement electrode pairs are near the injecting electrode pairs. The equipotential density is highest at the injecting electrodes locations that causes higher measured potentials distribution at the measurement electrode (see Figure 5.1 (B))

Figure 4.3 shows the potential distribution when inserting the tissue equivalent material in the phantom near the measuring electrodes. The tissue equivalent materials affect the conductivity distributions that cause the potential decreasing. The high conductivity area is represented by high current density lines (Lee E. Baker) that result in shifting of the equipotential lines near the tissue equivalent material. The decreased potential results from the shifted equipotential line as shown in Figure 4.3 (A-D). A large size of material affects the potential distribution greater than a small one, because a larges size means more surface area than a smaller size. A large surface leads to a high current density at the tissue equivalent material (a current line will enter the high conductivity materials). The equipotential line around that material would shift presenting a potential decreasing.

The tissue equivalent material is (edema and tumour lump) conductivity value is very important for validation model. The method that is used to preparing and setting the tissue conductivity is a complex method. Moreover, the conductivity of tissues depends on concentration and temperature of the saline solution. However, the preparation was performed in chemical lab with an instrument checking for accurate conductivity value.

Table 4.2, the potential distributions were measured by point electrode which was quite high at the locations at 40 and 140 degree. A current density around the injecting electrodes is high.

Table 4.3 shows the potential magnitude decreasing from normal level of 6.3 % approximately at $1cm^3$. A different volume of lump affects the potential distribution amplitude on the model. These findings suggest that a large size of edema lump is easily detected and measured. However, a system is used to detect the small size of edema should provide a higher gain and sensitivity.

The electrical impedance measurement system bases on electrical circuit and microcontroller (Appendix A). The measurement system was shown in the Figure 3.9. The prototype of electric impedance measurement was designed and constructed basing on an appropriate component in the country. Some component was imported from foreign countries (such as instrument amplifier).

The evaluation of the phantom model confirms that the edema lump on the finite element model causes to the potential distribution to be unsymmetrical depending on the location of the lesion.

CHAPTER VI
CONCLUSION

6.1 Conclusion

This study attempted to determine a suitable location of surface electrodes for bioelectrical measurement and predict the electric potential distribution by applying the finite element method to the 3D-head model generated from MRI images of a real patient with brain edema. It is well known that the electric potential distribution around an axis defined by a line between charge applying locations (electrodes) should be symmetric if brain's materials (CSF, tissues, and skull) are distributed evenly along the mentioned axis, which is generally the case. The FEM calculation results show that, in the case of brain edema, the potential distribution is not symmetric depending on the location of the lesion. Figures 4.1 (A) and (B) confirm this argument. The locations of charge applying electrodes are also essential in increasing detectable potential difference between two sides along the axis defined by a line between charge applying locations (electrodes). If charge applying electrodes are placed nearby the lesion region, the measured potential difference is higher (Figure 6, approximately 300 mV) than the case where they are not (Figure 4.1, approximately 100 mV). It can be concluded that more than 85 % of electric potential was attenuated through the skull. Furthermore, electric potential distribution in brain with edema is found to be asymmetric and depends on locations of the swelling region in brain. Simulation results show that the current applying electrodes should be placed nearby the swelling region to increase detectable potential differences.

The consistency check was designed to confirm the simulation results. Electrical impedance equipment, tissue-equivalent (edema and tumour lump), and phantom were designed for the validation. The experiment was performed by applying constant alternating current to the phantom. The potential distribution was measured around the phantom with a tissue-equivalent (representing edema and tumour lumps) located at various angles in the phantom. Opposite electrode data acquisition method was used to acquire the data from the phantom. This acquisition pattern was controlled by a microprocessor program (PIC18F458). The experimental results show that the

potential distribution decreases when the tissue-equivalent material is located near the measurement electrodes. The decreasing potential amplitude depends on the tissue-equivalent size. Furthermore, the potential distribution is attenuated by the shell of plaster (representing the skull layer).

From the experiment; the results are in substantial agreement with the FEM calculation results. The experimental result indicates that edema lump affects the potential distribution of the phantom model. The detectable potential is higher if the edema volume is larger. The electrical impedance measurement can detect the potential distribution on the phantom model with a plaster shell (representing the skull layer). Moreover, the validation results suggest that the electrodes placement should be over the edema location for injecting current electrode and near the lesion area for measurement electrodes.

6.2 Recommendation and Further Study

6.2.1 Anisotropic and heterogeneous model

This property is recommended for representing human brain.

6.2.2 Time-varying coefficients

The bioelectric impedance measurement method is normally used to measuring an impedance value that varies with time and changed volume in the tissue. For future study, time-varying equation should be used.

6.2.3 Potential distribution of a normal brain is recommended

A potential distribution on the human normal brain is important as reference value that is used for comparison purposes. The potential distribution on the human normal brain should be studied with the FEM in the further work.

REFERENCES

1. ศ.นพ. ชุศักดิ์ เวชแพทย์. การโมนิเตอร์หน้าที่สมองการอบรมสัมมนาวิชาการ เรื่อง “เครื่องมือแพทย์ในหอผู้ป่วยวิกฤติสำหรับพยาบาล”รุ่นที่ 4 ณ อาคารสถาบันวิจัยและพัฒนาวิทยาศาสตร์และเทคโนโลยี มหาวิทยาลัยมหิดล ; 2544
2. Barbara E. Lingwood, Kimble R. Dunster, Paul B. Colditz, Leigh C. Ward Noninvasive measurement of cerebral biompedance for detection of cerebral edema in the neonatal piglet. Brain Research. 2002;945: 97-105
3. Lee E. Baker. Application of the Impedance Technique to the Respiratory System. IEEE Engineering in Medicine and Biology Magazine. 1968; March: 50-52
4. Schoeller D. A., Kushner R. F.Determination of Body Fluids by the ImpedanceTechnique. IEEE Engineering in Medicine and Biology Magazine. 1989; March: 19-21.
5. Max E. Valentinuzzl, Julio C. Spinlli. Intracardiac Measurements with theImpedance Technique. IEEE Engineering in Medicine and Biology Magazine. 1989;March: 27-34.
6. Noninvasive technique. Impedance Plethysmography: theoretic, experimental and clinical considerations; p. 119-131
7. A T Tidsweel, A Gibson,R H Bayford, D S HolderElectrical impedance tomography of human brain activity with atwo-dimensional ring of scalp electrodes. Physiol. Meas. 2000; 22:167-175
8. Robert Paterson. The Biomedical Engineering Handbook.Second Edition. The electrical conductivity of tissues; P. 10-1 – 10-12

9. Tungjitkusolmum, S. , Haemmerich, D. , Ozkan, O.R. , Staelin S.T. ,Mahvi, D. M , Webster J.G. Change in electrical resistivity of swine liver after occlusion and postmortem. Medical & Biological Engineering & Computing 2002; 40: 29-33

10. Jang-Zern Tsai, James A. Will, Scott Hubbard-Van Stelle, Hong Cao, Supan Tungjitkusolmum, Young Bin Choy, Dieter Haemmerich, Vicken R. Vorporian, John G. Webster. In vivo measurement of swine myocardial resistivity, IEEE Trans, Biomed,Eng.2002; 49: 472-482

11. Jang-Zerm Taai, Hong Cao, Supan Tungjitkusolmum, Eung Je Woo, Vicken R. Vorperian, John G. Webster. Dependence apparent resistance of four-electrode probes insertion depth. IEEE Trans, Biomed,Eng. 2000; 47:41-48

12. Jang-Zerm Taai, James A. Will, Scott Hubbard-Van Stelle, Hong Cao, Supan Tugjitkusolmum, Young Bin Choy, Vicken R. Vorpirian, John G. Webster. IEEE Trans, Biomed,Eng. 2002; 49:484-494

13. L. Voo, S. Kumaresan, F. A Pintar, N. Yoganandan, A. Sances. Finite-element models of the human head. Med & Biol. Eng. & Comput.1996; 34: 375-381

14. M. Kacarska, L. Ololoska-Gagoska, S. Loskovaka, L. Grcev. Visualization of Induced Currents and SAR in Human's Head in Cellular Telecommumications. 1999; 0-7803-5639: 1012-1015

15. Youlin Geng, Xiuqin Zhu, Xinbao Wu, Peinan Jiao, Junmei Fan. The Distribution of Electromagenetic Field in Anisotropic Brain Tisue. 2000; 0-7803-6513-5: 205-206

16. Ernest L, Carter. JR, Vresilovic E. J, Solomon R, Pollack. R, Brighton. T. Carl. Field Distributions in Vertebral Bodies of the Rat During Electrical Stimulation. IEEE Transactions on Biomedical Engineering. 1989; 36:333-345

17. Ernest L, Carter. JR, Vresilovic E. J, Solomon R, Pollack. R, Brighton. T. Carl. Theoretical Determination of the Current Density Distributions in Human Vertebral Bodies During Electrical Stimulation. IEEE Transactions on Biomedical Engineering. 1990; 37: 606-614

18. Ducheyne Paul, Lisa Yost Ellis, Solomon R. Pollack, David Pienkowski, John M. Cuckier. Field Distributions in the Rat Tibia with and without a Porous Implant During Electrical Stimulation: A Parametric Modeling. IEEE Transactions on Biomedical Engineering. 1992; 39:11681178

19. Kamal P. Kothiyal, Balakrishnan Shankar, Lawrence J. fogelson, Nitish V. Thakor. Three-Dimensional Computer Model of Electric Fields in Internal Defibrillation. Proceedings of The IEEE. 1988; 76:720-730

20. Marc A. Camacho, John L. Lehr, Solomon R. Eisenberg. A Three-Dimensional Finite Element Model of Human Transthoracic Defibrillation: Paddel Placement and Size. IEEE Transactions on Biomedical Engineering. 1995; 42: 573-578

21. Weiping Wang, Solomon R. Eisenverg. A Three-Dimensional Finite Element Method for Computing Magnetically Induced Current in Tissues. IEEE Transactions on Magnetic. 1994; 30: 5015-5023

22. Atsuo Chiba, Katsuo Isaka. Dendity Distribution of Current Induced Inside The Brain in The Head Part of The Human Model Exposed to Power Frequency Electric Field. High Voltage Engineering Symposium Conference Publication. 1999; 467: 22-27

23. Jens Haueisen, Ceon Ramon, Michael Eiselt, Hartmut Brauer, Hannes Nowak. Influence of Tissue Resistivities on Neuromagnetic Fields and Electric Potentials Studied with a Finite Element Model of the Head. IEEE Transactions on Biomedical Engineering. 1997; 44:727-735

24. Vries P. M. J. M de, Meijer J. H., Vlaanderen K., Visser V., Oe P. L, De P. L, Donker A. J. M and Schneider. H. Measurement of transcellular fluid shift during haemodialysis. Medical & Biological Engineering & Computing. 1989; 27, 152-158.

25. Thom F. Oostendorp, Jean Delbeke and Dick F. Stegeman. The conductivity of the human skull: results of In Vivo and In Vitro measurements. IEEE Transactions on Biomedical Engineering. 2000; 47: 1487-1492

APPENDIX

APPENDIX A

Electrical Impedance Measurement Design and Construction

This section described the design and construction of electrical impedance tomography (EIT). The EIT was designed base on microprocessors controller. The measurement technique is based on a conventional four-electrode impedance measurement system. The system was summarized in Figure 3.9. This system consists of eight parts: sine wave oscillator, voltage-to-current converter (V/I), multiplexer (MUX), 32-electrodes, digital coupler, amplifier, demodulator and microcontroller. The basic operation of each part was described as following.

A sinusoidal waveform with 100 KHz frequency is generated by a sine wave oscillator. The signal is amplified and then sent to the voltage to constant current source (VCCS). The VCCS converts the voltage from oscillator to a constant current source. Switch current value are provided in this part. There are 100 uA, 500 uA, 1 mA, 2 mA, 3 mA, 4 mA, 5 mA, 6 mA , 7 mA , 8 mA, 9 mA, 10 mA. A sinusoidal current is applied between a pair of electrodes by means of analog multiplexers. The potential values on the object is detected by measurement electrodes which made by using analog demultiplexers. These values are amplified by an instrumentation amplifier with high gain and filed the 50 Hz from AC line by filter. The demodulator is used to separate the real and imaginary parts from signal. The operating of system is controlled by microcontroller. It provides measurement protocol and transferring the data to PC. Different block of the design are described below:

1 Sine wave Generator Part

MAX 038 is a high-frequency waveform generator that used to generate the sine wave as illustrated in Figure 2. It consists of 2 units as generator and amplifier. It can produce low-distortion sine, triangle, saw tooth, and square waveform. The waveform can select by setting pins A0 and A1.

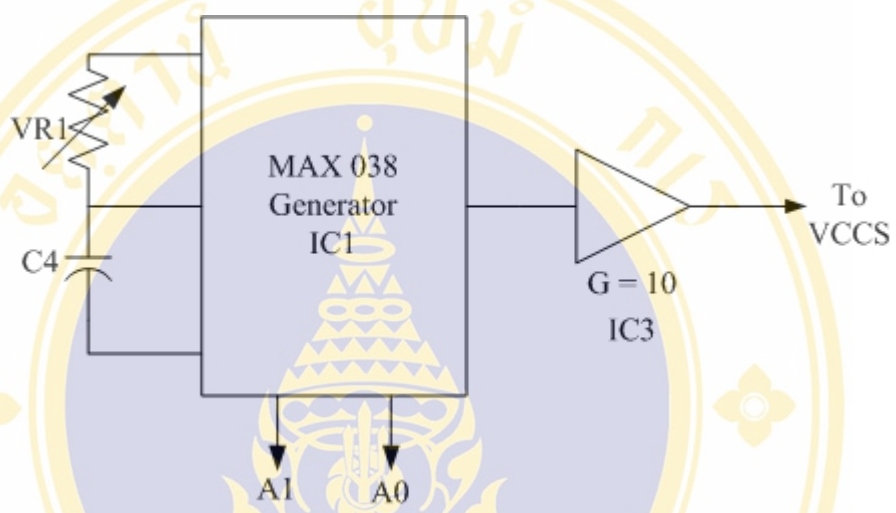

Figure A.1 Sine wave generator block diagram

Variable resistor VR1 and capacitor C4 combined with MAX038 generated the 100 KHz sine wave at output pin. The signal is passed to buffer amplifier to provide output impedance. After that, the signal is passed to amplifier circuit. The IC3 is an amplifier that combines with resistors to provide amplifier gain. The 20 Vp-p sine wave is produced by these amplifier. And then, it send to voltage constance current source (VCCS).

2 Voltage-controlled current source (VCCS) part

The VCCS have high output impedance due to a closed–loop feedback system that converts the voltage to current. The circuit is divided two parts as a unit gain amplifier and series resistor.

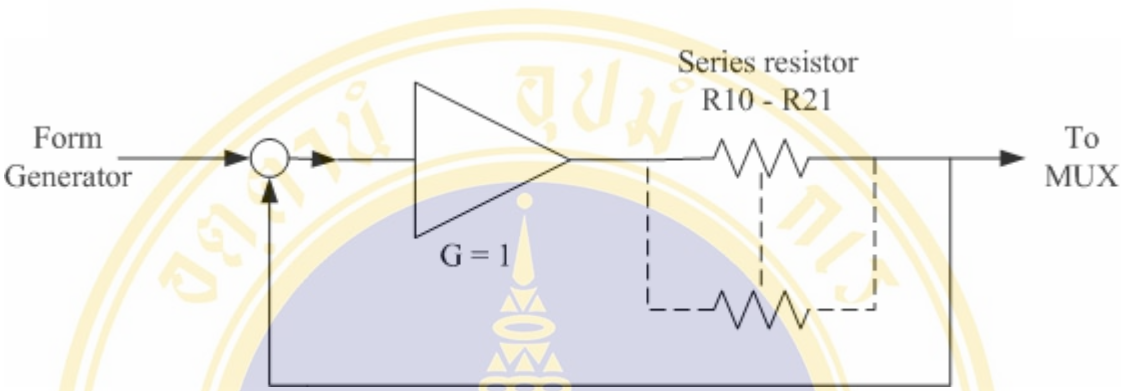

Figure A.2 Voltage-controlled current source block diagram

3 Analog Multiplexer (MUX) part

An analog multiplexer consists of two parts: MUX for current injection electrode and MUX for voltage measurement electrode. The output of VCCS will send through current injection electrodes. The current can be switched between different electrode pairs by means of analog multiplexers. The voltage on object is also measured by switching of analog multiplexer which connects to the instrumentation amplifier. The measurement protocol is defined by PIC microcontroller program.

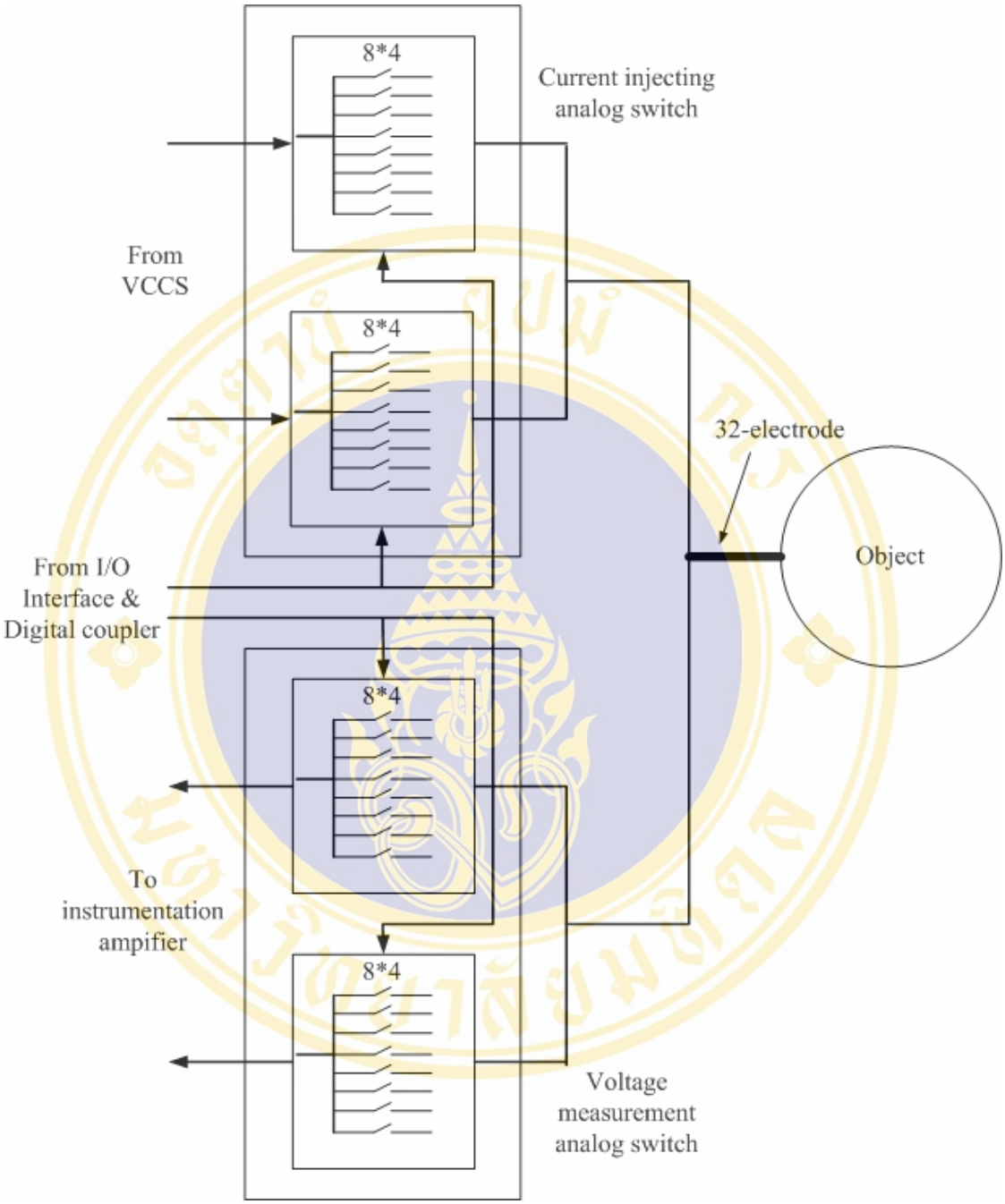

Figure A.3 An analog multiplexer block diagram

For analog multiplexer, 8-channal high performance analog multiplexer and low cast, MAX DG508 is used. It has low switching time, typical 1 uS. The system block diagram is shown in Figure A.3.

4 Amplifier Circuit Part

The potential on the object is passed through demultiplexer switch after that send to an amplifier past. The amplifier is instrumentation with high gain, high CMRR and high input impedance. Analog Device AD 524, easy designed, is used. Those potential is amplified that passes to an isolation amplifier for separating the patent from system for safety requirements. To selecting frequency range and ejecting unwanted signals, high pass and 50 Hz filter are used after that, and then passes these signals through quadrature demodulater.

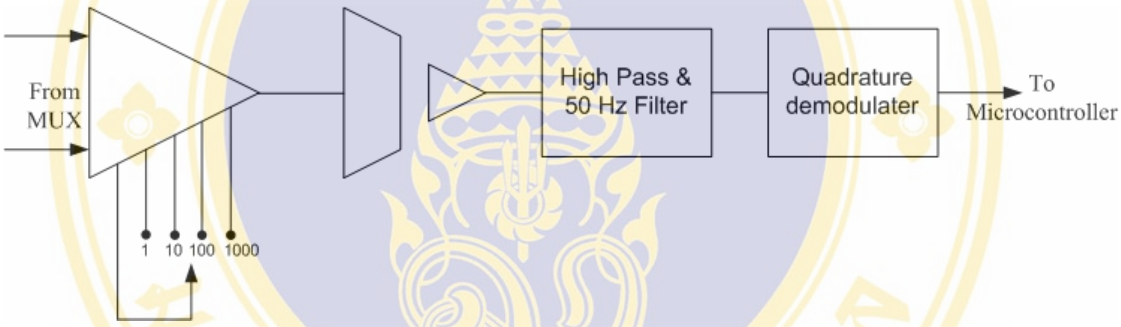

Figure A.4 An amplifier block diagram

5 I/O Interface

The digital interface part is used primarily to provide isolate between the system and the microcontroller. Digital outputs of the PIC microcontroller which controls the analog multiplexers are isolated by using a digital coupler. The digital have a small delay time.

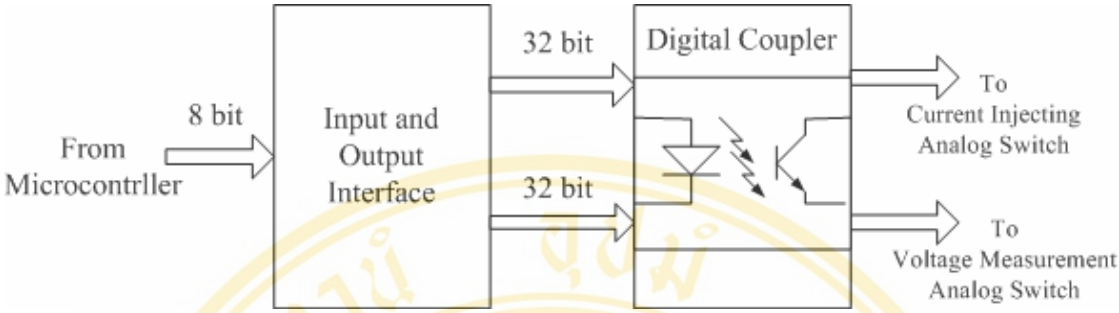

Figure A.5 Input and output interface block diagram

6 Microcontroller Part

The microcontroller part' s function is to manage the operation of analog multiplexer, measurement the amplitude and phase of signal, display the operation of system, and transfer the data to PC computer, etc. PIC 18F458 Microcontroller is used as microcontroller unit. It is a 8 bit wide data microcontroller which has many built-in peripherals components such as timer/counter, 32 K bytes flash memory, 256 bytes EEPROM, 1 serial communication port and analog to digital converter. Consequently, it can reduce amount of external components connected to it

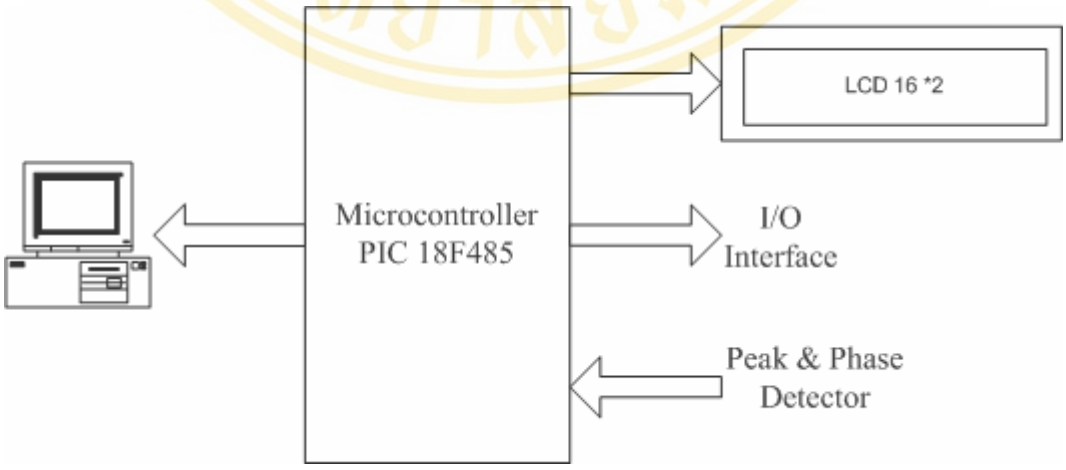

Figure A.6 A microcontroller block diagram

7 The power supply part

The function of power supply part is to convert 220 VAC, 1 Amps into many ranges of DC regulated output using convention regulated linear voltage circuit. The ranges of DC output level depend on consumed parts as follow:

- +/- 5 volts supply for digital interface, sine wave generator, VCCS and microcontroller part
- +/- 12 volts supply for amplifier circuit part
- +/- 15 volts supply for analog multiplexer part

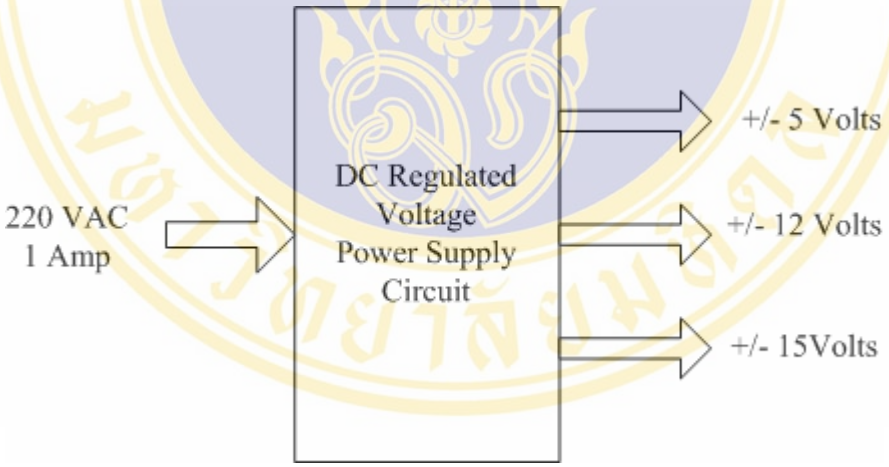

Figure A.7 A power supply block diagram

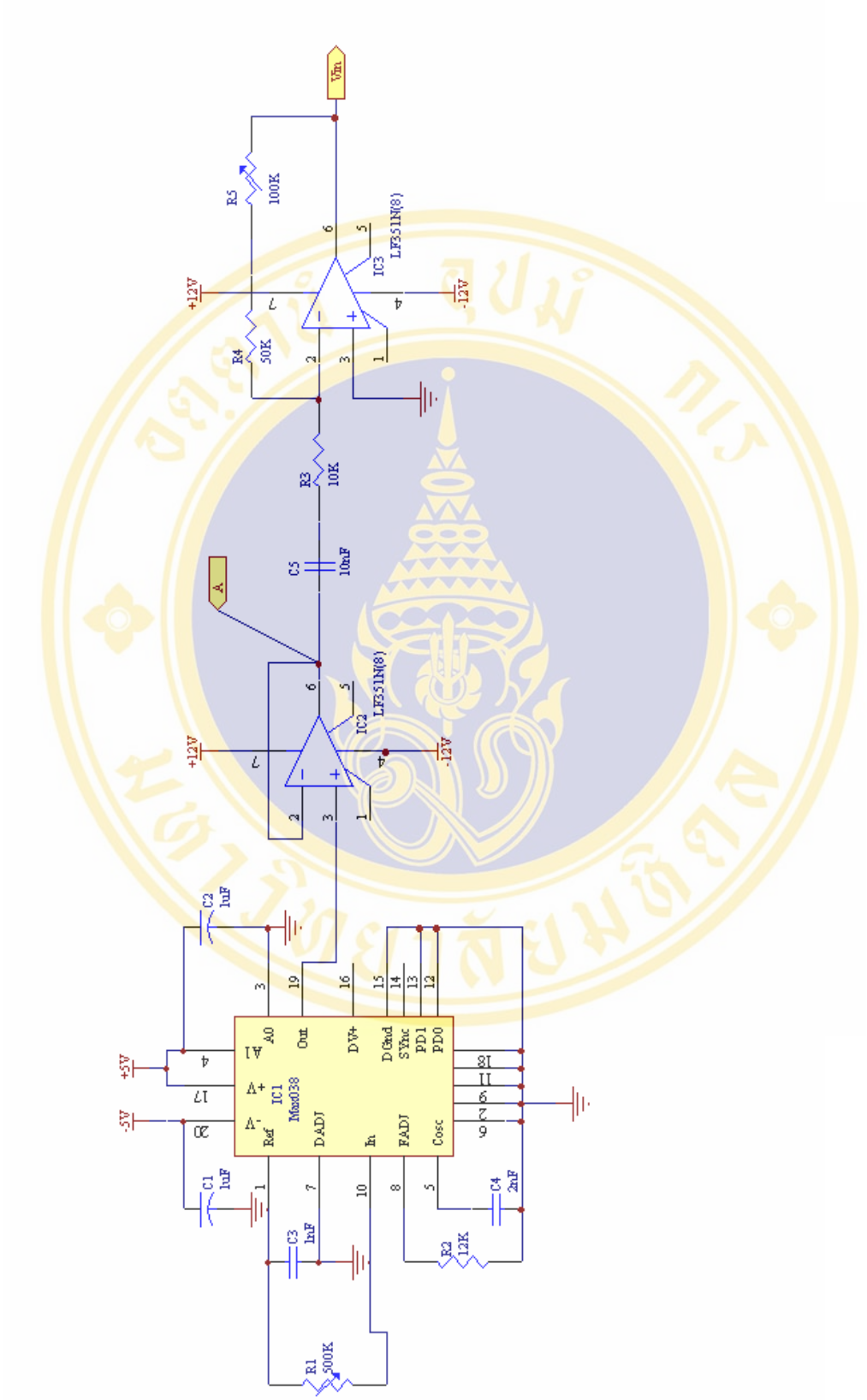

Figure A.8 A schematic diagram of sine wave generator circuit

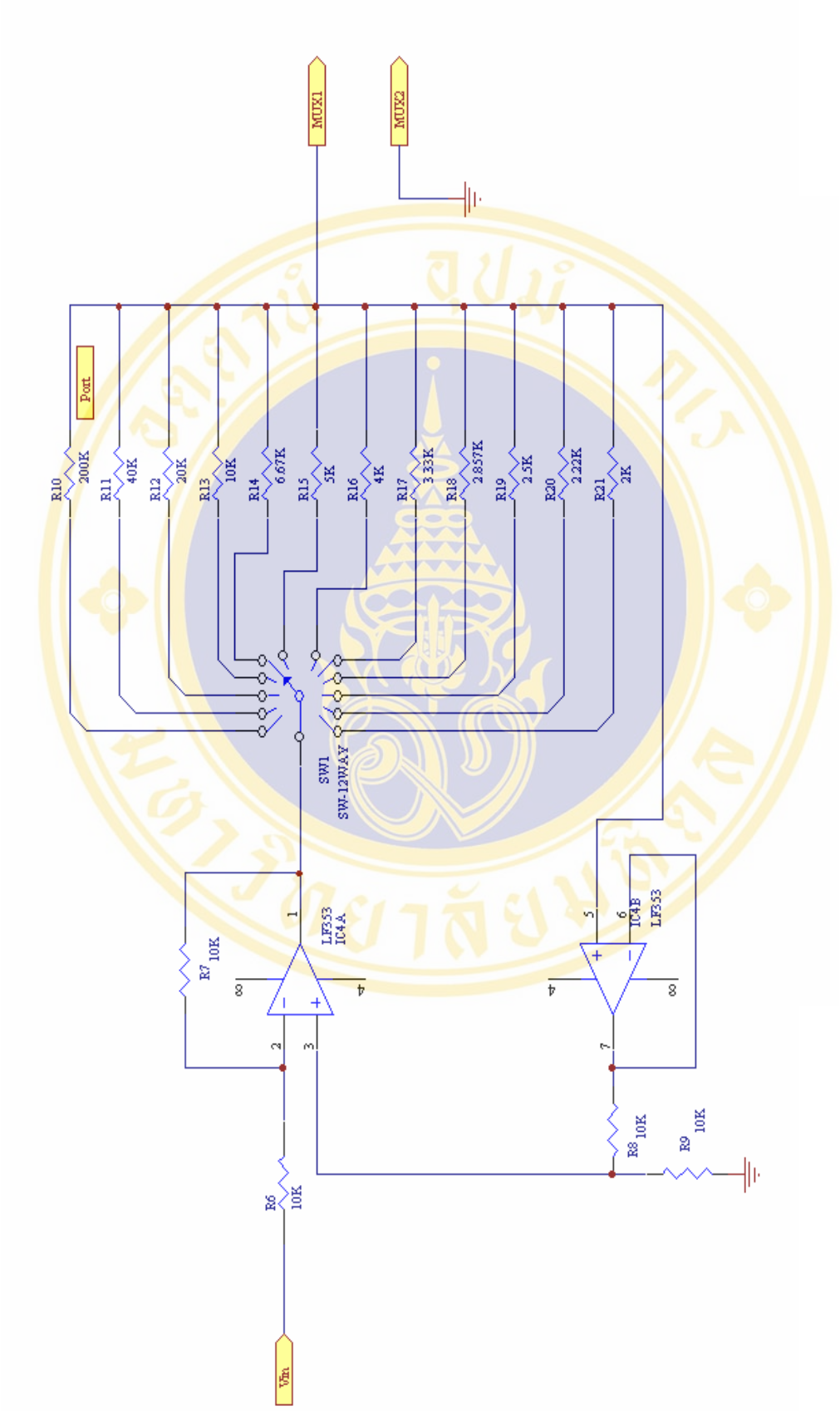

Figure A.9 A schematic diagram of voltage-controlled current source (VCCS) circuit

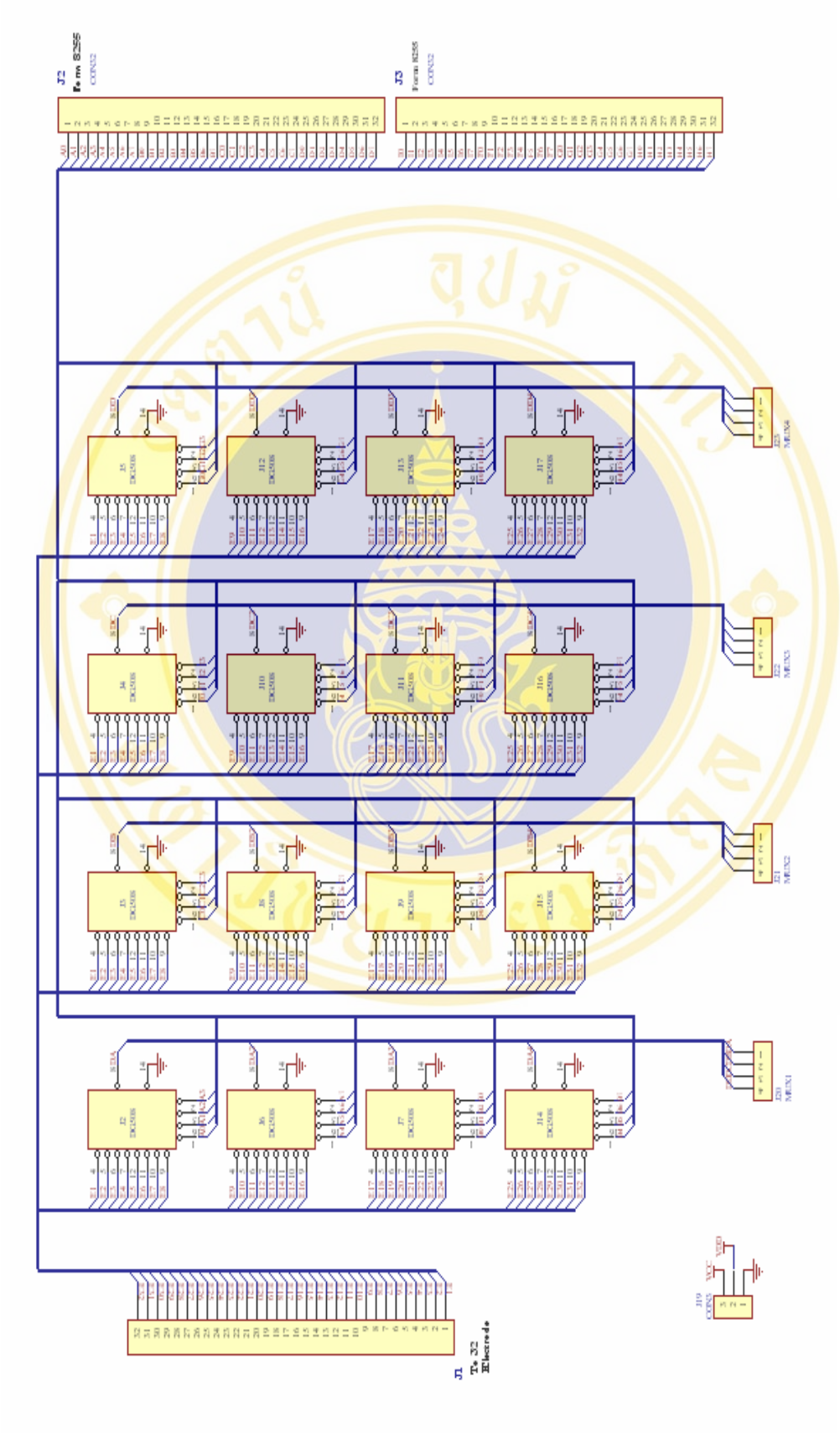

Figure A.10 A schematic diagram of analog multiplexer (MUX) circuit

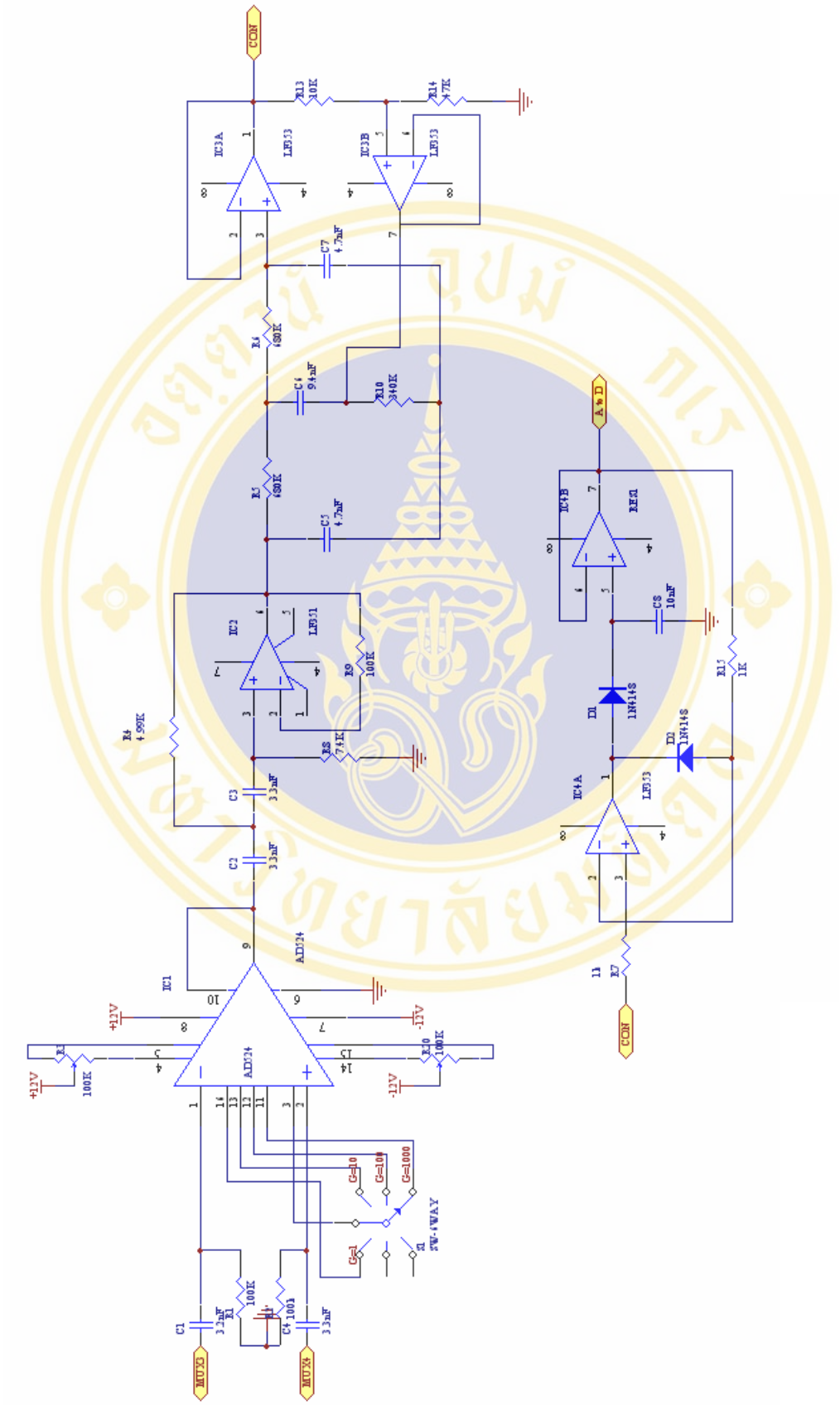

Figure A.11 A schematic diagram of amplifier circuit

APPENDIX B

This section describes the process for preparing saline and tissue equivalent material which used to validation process. Equipment is specially designed to check the conductivity of the tissue equivalent material which indults in this section.

1. Preparing saline conductivity

Saline with known conductivity was used to prepare the layers. The saline was prepared from sodium chloride and deionization water. There are three saline conductivity which were prepared. These saline's conductivity were measured 1.42×10^{-3}, 6.25×10^{-3} and 4.34×10^{-3} Ω/cm, respectively. The concentration of saline were 0.0276 molar at 680 ml, 0.034 molar at 920 ml, 0.159 molar at 628 ml for white mater, blood and tumour conductivity, respectively. Conductivity meter (Inolap cond level 2, Model Tetracon 326) was employed to confirm measured conductivity value of each saline. Five gram of agar powder was added into those salines.

2. Saline cooking

The saline with agar powder prepare previous processes was cooked to make conductivity of edema lump. This process needs an equipment which specially designed to check the conductivity because it is hot and not liquid. Four-electrode method was applied to check the conductivity of saline while it cooking. The four-electrode method system is shown in Figure B.1. This method has been used by *Supan el at* for measurement of swine myocardial (10). The system consists of probes, measurement circuit and equipment. The probes were made of four stainless steel needles, whose outer diameter was 0.41 mm. The four electrodes were deployed in a linear array held to an epoxy base.

The measurement circuit was differential amplifier and current-to-voltage. Function generator and oscilloscope were used to feed a sine wave signal and measure output signal. The receptivity can be directly calculated from four-electrode method by using the following equation.

$$\rho = Ra \times Kp \quad (A.1)$$

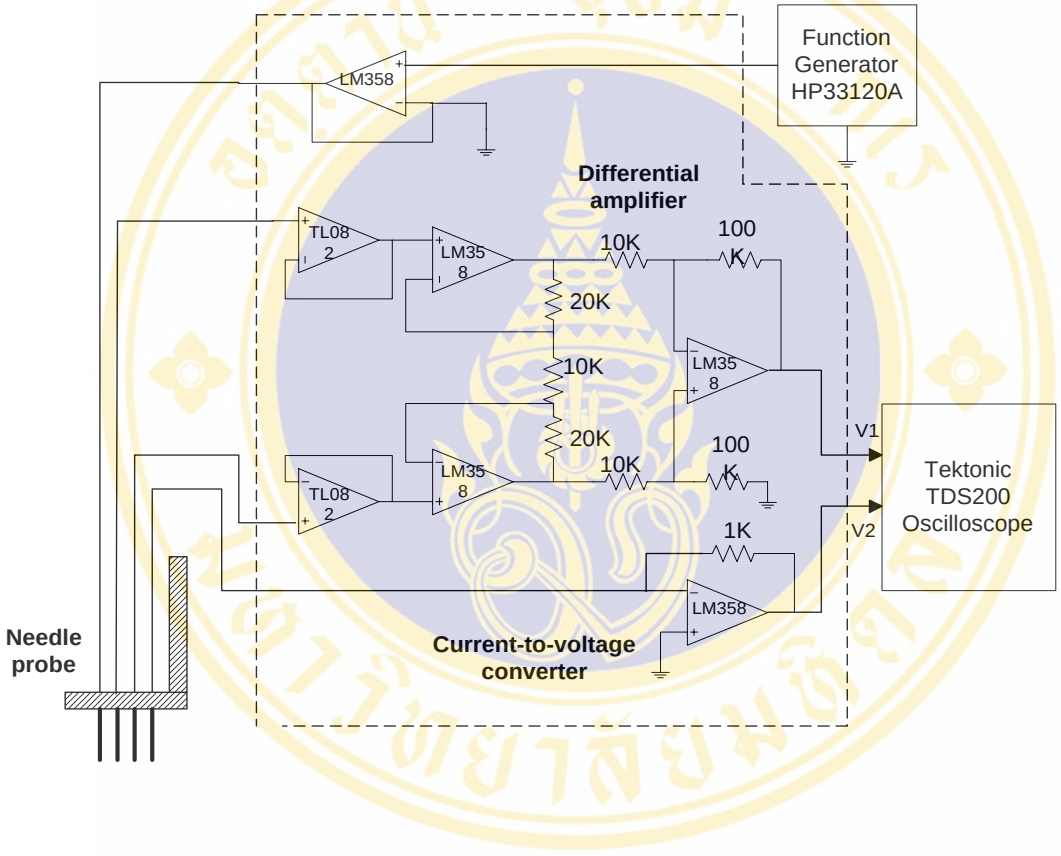

Figure B.1. Four-electrode system use for measurement the saline conductivity

where Ra, the apparent resistance, is the ratio of the voltage difference sensed by the two voltage electrode and the current delivered and collected by two current electrodes and Kp , the probe constant, is the ratio of the tissue resistivity divided by the apparent resistance. The probe constant is determined by the electrode configuration of the resistivity probe and is measured by calibration with a reference material. The conductivity of tissue can be calculated from the resistivity of tissue (14).

3. Calibration and resistivity measurement procedure

The resistivity measurement is performed in following steps:

Step 1. Measuring the oscilloscope-circuit constant.

The oscilloscope-circuit constant Ko-c is calculated by equation.

$$(K_{o-c})_1 = \frac{(Rf)_1}{(V_1 / V_2)_1} \quad \text{(A. 2)}$$

The calibration uses a resistance (Rf), which equal to the saline resistivity of the preparing saline conductivity section. Firstly, Rf was measured by a multimeter, recorded the resistant value. Then added two other resistor and connected to the four terminals of the measurement circuit as shown in Figure 14(a), and measured the voltages (V1,V2). After that the Rf , V1 and V2 were inserted in equation 14 to find oscilloscope-circuit constant $(Ko\text{-}c)_1$.

Step 2). Measuring the saline resistivity.

The saline solution prepared in lab was measured with a syringe tube with four silver wires penetrating through the tube as shown in Figure B.2 (b). The measured saline resistivity was

$$(\rho_s)_2 = (\frac{V_1}{V_2})_2 (K_{o-c})_1 (\frac{A}{d})_2 \quad \text{(A.3)}$$

where A is the inner cross-sectional area of the syringe tube and *d* is the voltage electrode distance. The nominal value of A was 1.54 cm^2 and of d is 3 cm. The distance between the current electrodes and its adjacent voltage electrode is 1 cm.

In (15), the oscilloscope-circuit constant (Ko-c) measured in Step 1 was used. We used the same circuit and the same oscilloscope in all steps.

Step 3). Measuring the wire-probe constant.

The wire-probe constant (Kw-p) is calculated by.

$$(K_{w-p})_3 = \frac{(\rho_s)_2}{(\frac{V_1}{V_2})_3 (K_{o-c})_1} \quad \text{(A.4)}$$

The wire-probe constant was performed on cylindrical plastic cup as shown in Figure 14(c). First, the saline in step 2 was prepared in the cup, then the voltage (V_1,V_2) were measured by the needle probe electrode. After that, the oscilloscope constant valve in Step 1, the saline resistivity value in Step 2 and voltage (V_1,V_2) were inserted in the

equation number16 to calculate the wire-probe constant. We corrected the measured saline resistivity with a –2% /°C temperature coefficient in these experiment.

Step 4). Measuring the agar gel resistivity.

The needle electrode was inserted into the agar gel saline to measure the resistivity. Using the oscilloscope-circuit constant Ko-c measured in Step1, the wire-probe constant Kw-p measured in Step 3, and the output ratio V_1/V_2 of the oscilloscope measured in this step.

$$(\rho_r)_4 = (\frac{V_1}{V_2})_4 (K_{o-c})_1 (K_{w-p})_3 \qquad (A.5)$$

The equation (A.4) was used to determine the agar gel saline while it cooking. After it congeals following cooking, It was measured the resistivity of the agar with a four-electrode needle probe with known probe constant performed in Step 3. If the resistivity deviated from the desired value, water or 1 molla of sodium chloride solution was added and then cooked the mix again. This process was repeated until we attain the desired resistivity.

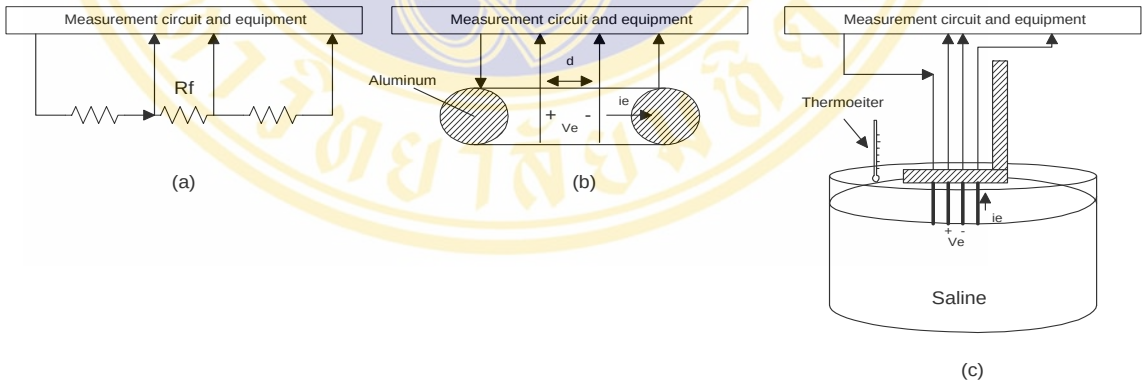

Figure B.2 The configuration used in Step 1-3. (a) The configuration for measuring the oscilloscope-circuit constant Ko-c in Step 1. (b) The configuration for measuring the saline resistivity in Step 2. (c) The configuration for measuring the wire-probe constant Kw-p in Step 3.

Note that the subscript next to a parenthesis represents the step number in which the quantity inside the parenthesis was measured or was pertinent to the configuration used.

BIOGRAPHY

NAME	Mr. Pracha Yambangyang
DATE OF BIRTH	18 January 1973
PLACE OF BIRTH	Samut Sakhon, Thailand
INSTITUTIONS ATTENDED	King Mongkut's Institute of Technology North Bangkok, 1995-1998 Bachelor of Science (Electrical Engineering) Mahidol University, 2001-2004 Master of Engineering (Biomedical Engineering)
POSITION&OFFICE	Biomedical Instrument Division Faculty of Medicine Siriraj Hospital Tel 02-4197561
HOME ADDRESS	272/41 Moo 1 Lug-Sam Bang-Pao Samut-Sakhon E-mail:srpyb@mahidol.ac.th